

# Investigating the effect of El Niño on nitrous oxide distribution in the Eastern Tropical South Pacific

Qixing Ji<sup>1</sup>, Mark A. Altabet<sup>2</sup>, Hermann W. Bange<sup>1</sup>, Michelle I. Graco<sup>3</sup>, Xiao Ma<sup>1</sup>, Damian L. Arévalo-Martínez<sup>1</sup>, and Damian S. Grundle<sup>1,4</sup>

<sup>1</sup>GEOMAR Helmholtz Centre of Ocean Research Kiel, Kiel, 24105, Germany

<sup>2</sup>School for Marine Science & Technology, University of Massachusetts Dartmouth, New Bedford, Massachusetts, USA

<sup>3</sup>Dirección General de Investigaciones Oceanográficas y cambio Climático, Instituto del Mar del Perú (IMARPE), P.O. Box 22, Callao, Perú

<sup>4</sup>Bermuda Institute of Ocean Sciences, St. George's, GE01, Bermuda

*Correspondence to:* Qixing Ji (qji@geomar.de)

**Abstract.** The open ocean is a major source of nitrous oxide (N<sub>2</sub>O), an atmospheric trace gas attributable to global warming and ozone depletion. Intense sea-to-air N<sub>2</sub>O fluxes occur in major oceanic upwelling regions such as the Eastern Tropical South Pacific (ETSP). The ETSP is influenced by the El Niño-Southern Oscillation that leads to inter-annual variations of physical, chemical and biological properties [in the water column](#). In October 2015, a strong El Niño event was developing in the ETSP; we conduct field observation to investigate (1) the N<sub>2</sub>O production pathways and associated biogeochemical properties, and (2) the effects of El Niño on water column N<sub>2</sub>O distributions and fluxes using data from previous non-El Niño years. Analysis of N<sub>2</sub>O natural abundance isotopomers suggested that nitrification and partial denitrification (nitrate and nitrite reduction to N<sub>2</sub>O) were occurring in the near surface waters; indicating that both pathways contributed to N<sub>2</sub>O effluxes. Higher than normal sea surface temperatures were associated with a deepening of the oxycline and the oxygen minimum layer. Within the shelf region, surface N<sub>2</sub>O supersaturation was nearly an order of magnitude lower than those of non-El Niño years. Therefore, a significant reduction of N<sub>2</sub>O efflux (75 – 95 %) in the ETSP occurred during the 2015 El Niño. At both offshore and coastal stations, the N<sub>2</sub>O concentration profiles during El Niño showed moderate N<sub>2</sub>O concentration gradients, and the peak N<sub>2</sub>O concentrations occurred at deeper depths during El Niño years; this was likely the result of suppressed upwelling retaining N<sub>2</sub>O in subsurface waters. [At multiple stations](#), water-column inventories of N<sub>2</sub>O within the top 1000 m were up to 160% higher than those measured in non-El Niño years, indicating that subsurface N<sub>2</sub>O during El Niño could be a reservoir for intense N<sub>2</sub>O effluxes when normal upwelling is resumed after El Niño.

## 1 Introduction

The El Niño-Southern Oscillation (ENSO) is a naturally occurring decadal climate cycle that affects the oceanic and atmospheric conditions across the equatorial Pacific (Philander, 1983). A pronounced effect of ENSO in the ocean is the

redistribution of heat flux across the tropical and subtropical Pacific. Generally, the ENSO cycle can be divided into three phases, El Niño, La Niña and neutral. During El Niño / La Niña years, higher / lower sea surface temperature and deepening / shoaling of the thermocline depth occur in the Eastern Tropical South Pacific (ETSP) (Barber and Chavez, 1983). During El Niño years, upwelling is suppressed in the ETSP, and thus reducing upward nutrient fluxes to the surface waters causing decreased primary production (Chavez et al., 2003; Niquen and Bouchon, 2004; Graco et al., 2017).

The ETSP is an oceanic region with intense sea-to-air flux of nitrous oxide ( $\text{N}_2\text{O}$ ), a strong greenhouse gas and a potent ozone depleting agent in the 21<sup>st</sup> century (Ravishankara et al., 2009). Diverse microbial processes involved in the production and consumption of  $\text{N}_2\text{O}$  occur in the ETSP, a major oceanic oxygen minimum zone (OMZ) having wide range of  $\text{O}_2$  concentrations spanning sub-nanomolar level at intermediate depths (Revsbech et al., 2009) to atmospheric saturation at the surface. In the presence of oxygen,  $\text{N}_2\text{O}$  is a by-product during the first step of nitrification, i.e. ammonium ( $\text{NH}_4^+$ ) oxidation to nitrite ( $\text{NO}_2^-$ ) (Anderson, 1964). Under suboxic and anoxic conditions,  $\text{N}_2\text{O}$  is produced via partial denitrification, i.e.  $\text{NO}_2^-$  reduction and nitrate ( $\text{NO}_3^-$ ) reduction (Codispoti and Christensen, 1985). Partial denitrification can be mediated by denitrifying bacteria using  $\text{NO}_2^-$  and  $\text{NO}_3^-$  as substrates, as well as nitrifying bacteria using only  $\text{NO}_2^-$ , a process termed nitrifier-denitrification (Frame and Casciotti, 2010; Trimmer et al., 2016). The dominant biological sink of  $\text{N}_2\text{O}$  in the ocean is the last step of denitrification where  $\text{N}_2\text{O}$  is reduced to  $\text{N}_2$  under anoxic conditions (Codispoti and Christensen, 1985). Recent investigations suggest that  $\text{N}_2\text{O}$  uptake by diazotrophs is another possible  $\text{N}_2\text{O}$  sink occurring at the surface waters (Farías et al., 2013; Cornejo et al., 2015). Its environmental significance awaits further exploration.

Research on the impact of ENSO on  $\text{N}_2\text{O}$  dynamics was initiated by the observation of significant reduction in oceanic  $\text{N}_2\text{O}$  effluxes during El Niño events (Cline et al., 1987; Butler et al., 1989). Recent model simulations demonstrated that ENSO events could induce lower denitrification rates, higher nitrification rates and lower  $\text{N}_2\text{O}$  fluxes (Mogollón and Calil, 2017; Yang et al., 2017), which could be related to changes in  $\text{O}_2$  and organic matter availabilities that are critical environmental factors regulating  $\text{N}_2\text{O}$  production (Elkins et al., 1978; Farías et al., 2009; Arévalo-Martínez et al., 2015; Kock et al., 2016). Here we report water column hydrography, nitrogen biogeochemistry and  $\text{N}_2\text{O}$  distribution during October 2015 when a strong El Niño event (recurrence interval > 10 years) was developing (Stramma et al., 2016; Santoso et al., 2017). The natural abundance isotopomers of  $\text{N}_2\text{O}$ , i.e. the intramolecular configuration of stable isotopes ( $^{15}\text{N}$  vs.  $^{14}\text{N}$  and  $^{18}\text{O}$  vs.  $^{16}\text{O}$ ) were used to determine the pathways of  $\text{N}_2\text{O}$  production and consumption by a simple mass balance model outlined previously (Yamagishi et al., 2007; Grundle et al., 2017). Finally, the effects of a strong El Niño event on the surface and water column  $\text{N}_2\text{O}$  distributions were investigated by incorporating archived ETSP datasets that demonstrated contrasting hydrography and biogeochemistry between El Niño and non- El Niño years.

## 2 Materials and Methods

### 2.1 Field sampling and laboratory measurements

The progress and the strength of El Niño was quantified by the Ocean Niño Index (ONI, Figure 1), defined as the running 3-month average sea surface temperature anomaly for the Niño 3.4 region in the east-central tropical Pacific (5°S – 5°N, 120°W – 170°W). The 2015-16 El Niño was a “strong El Niño event” indicated by  $ONI \geq 0.5$  °C from November 2014 to May 2016. This study was conducted on the ASTRA-OMZ SO243 cruise on board the R/V *Sonne* between the 5<sup>th</sup> and 22<sup>nd</sup> October 2015 from Guayaquil, Ecuador to Antofagasta, Chile (Figure 2a). In October 2015, the El Niño was still developing with  $ONI = 2.1$  °C, comparable to other strong El Niño events in 1972-73, 1982-83, 1997-98 (Stramma et al., 2016).

The sampling stations are categorized into offshore (Figure 2a in red polygon) and coastal (Figure 2a white polygon) according to their respective water depth: The coastal stations are shallower than 250 m whereas the offshore stations are > 3000 m in depth. Water samples were taken from a 24 × 10L-bottle CTD-rosette system. At every station, CTD-Niskin bottles collected water samples at 10 – 20 depths spanning the observed oxygen concentration range. The CTD system was equipped with two independent sets of sensors for temperature, conductivity (salinity) and oxygen measurements. Calibration for temperature, salinity and oxygen measurements were reported previously, with standard deviations of 0.002°C, 0.0011 PSU, and 0.8 µmol L<sup>-1</sup> [O<sub>2</sub>], respectively (Stramma et al., 2016). The detection limit of dissolved oxygen was ~ 3 µmol L<sup>-1</sup>; the oxygen deficient zone (ODZ) was operationally defined as water parcels with [O<sub>2</sub>] < 5 µmol L<sup>-1</sup>, and the upper and lower oxycline boundary layer was defined as [O<sub>2</sub>] = 20 µmol L<sup>-1</sup> isoline occurring above and below the ODZ, respectively. Saturation level of O<sub>2</sub> was calculated with in situ temperature and salinity according to Garcia and Gordon (1992). Dissolved NO<sub>3</sub><sup>-</sup> and NO<sub>2</sub><sup>-</sup> concentrations were measured at sea with an auto-analyzer (QuAatro, Seal Analytical, Germany). Chemical analyses of NO<sub>3</sub><sup>-</sup> and NO<sub>2</sub><sup>-</sup> had detection limit of 0.1 and 0.02 µmol L<sup>-1</sup>, respectively. For N<sub>2</sub>O concentration measurements, triplicate samples were collected in 20 mL brown glass vials and were crimp-sealed with butyl stoppers and aluminum caps. Immediately following this, a 10 mL helium headspace was created and 50 µL of saturated mercuric chloride (HgCl<sub>2</sub>) solution was added. After an equilibration period of at least 2 hours, the headspace sample (10 mL) was measured by a gas chromatograph equipped with an electron capture detector (GC/ECD) that was calibrated on a daily basis using dilutions of two standard gas mixtures. The detailed GC/ECD setup and calculation of N<sub>2</sub>O concentration were reported previously (Walter et al., 2006; Kock et al., 2016). For the N<sub>2</sub>O concentration data of the 2015 cruise, the standard deviation of triplicate sampling was 1 – 8 %, generally < 2.5 nmol L<sup>-1</sup>.

Water column N<sub>2</sub>O saturation was quantified by the N<sub>2</sub>O excess ( $\Delta N_2O$ ), defined as the concentration difference between measured and equilibrium values:

$$\Delta N_2O = [N_2O]_{measured} - [N_2O]_{equilibrium} \quad (1)$$

The N<sub>2</sub>O equilibrium concentration was calculated according to Weiss and Price (1980) with in situ temperature, salinity and the atmospheric N<sub>2</sub>O dry mole fraction in the year of 2015, 328 ppb at 1 atmospheric pressure (Blasing, 2016). The N<sub>2</sub>O efflux from the ocean to the atmosphere was calculated as the product of N<sub>2</sub>O excess and gas transfer coefficient ( $k_w$ , cm hr<sup>-1</sup>) that was derived according to empirical relationship proposed by Wanninkhof (2014):

$$k_w = 0.251 \times U_{10}^2 \times (Sc/660)^{-0.5} \quad (2)$$

where  $U_{10}$  denotes wind speed (m s<sup>-1</sup>) at 10 m above sea surface,  $Sc$  denotes the Schmidt number for N<sub>2</sub>O under in situ temperature (Wanninkhof, 2014).

Samples for natural abundance N<sub>2</sub>O isotopes and isotopomers were collected in 160 mL glass serum bottles with butyl stoppers and aluminum seals, and preserved with 100  $\mu$ L of saturated HgCl<sub>2</sub>. Isotopomeric measurements of N<sub>2</sub>O were carried out at the University of Massachusetts Dartmouth following procedures previously reported (Grundle et al., 2017). In brief, dissolved N<sub>2</sub>O was extracted by an automated purge-and-trap system and concentrated with liquid nitrogen. Interfering molecules such as H<sub>2</sub>O and CO<sub>2</sub> were isolated from N<sub>2</sub>O to increase measurement precision. A multi-collector isotope ratio mass spectrometer detected intact N<sub>2</sub>O molecule's mass ratio of 45/44 and 46/44 and NO<sup>+</sup> fragment's mass ratio 31/30. Relative abundance of N<sub>2</sub>O isotopomers were expressed using the delta notation ( $\delta X$ ), defined as the relative difference between isotopic ratio (R) of sample and reference material:

$$\delta X = \frac{R_{sample}}{R_{reference}} - 1 \quad (3)$$

where X denotes <sup>15</sup>N <sub>$\alpha$</sub> , <sup>15</sup>N <sub>$\beta$</sub>  and <sup>18</sup>O, R denotes the <sup>15</sup>N/<sup>14</sup>N at the central ( $\alpha$ ), terminal ( $\beta$ ) nitrogen positions and <sup>18</sup>O/<sup>16</sup>O at oxygen position of the N<sub>2</sub>O molecule. The value of  $\delta X$  is expressed as permil (‰) deviation relative to a set of reference materials: atmospheric N<sub>2</sub> for  $\delta^{15}N_{bulk}$ ,  $\delta^{15}N_{\alpha}$  and  $\delta^{15}N_{\beta}$  (Mohn et al., 2014), and Vienna standard mean ocean water (VSMOW) for  $\delta^{18}O$ . Therefore, mass ratios of 45/44, 46/44 and 31/30 determined  $\delta^{15}N_{bulk}$  (conventionally  $\delta^{15}N$ ),  $\delta^{18}O$ , and  $\delta^{15}N_{\alpha}$ , respectively. The  $\delta^{15}N_{\beta}$ , the relative abundance of N<sub>2</sub>O molecule with <sup>15</sup>N substitution at terminal ( $\beta$ ) position, was calculated by  $\delta^{15}N_{\beta} = 2 \times \delta^{15}N_{bulk} - \delta^{15}N_{\alpha}$ . Site preference (SP) are defined as follows:

$$SP = \delta^{15}N_{\alpha} - \delta^{15}N_{\beta} \quad (4)$$

Calibration of  $\delta^{15}N_{\alpha}$ -N<sub>2</sub>O,  $\delta^{15}N_{\beta}$ -N<sub>2</sub>O and  $\delta^{18}O$ -N<sub>2</sub>O was accomplished using four certified standard gases (supplied by Joachim Mohn, [see supplementary table S2](#)) encompassing the values reported here. The analytical precision of isotope measurements were  $\pm 0.07$ , 0.17, 0.36 and 0.18‰ for  $\delta^{15}N_{bulk}$ -N<sub>2</sub>O,  $\delta^{15}N_{\alpha}$ -N<sub>2</sub>O,  $\delta^{15}N_{\beta}$ -N<sub>2</sub>O and  $\delta^{18}O$ -N<sub>2</sub>O, respectively.

## 2.2 Additional datasets

The twice-weekly, 50-km resolution of sea surface temperature anomaly from NOAA's Satellite Coral Bleaching Monitoring Datasets (<https://coralreefwatch.noaa.gov/satellite/methodology/methodology.php>) were used to quantify the sea-surface temperature difference of the ETSP during October 2015 relative to 1985 – 1993. For N<sub>2</sub>O flux calculations,

instantaneous wind speed data at each of our sampling locations were acquired from shipboard metrological measurements. Seawater N<sub>2</sub>O and oxygen concentrations from previous sampling campaigns in the ETSP were extracted from the MEMENTO database (Kock and Bange, 2015). Specifically, data from the following cruises were used for comparison between El Niño and non-El Niño years: NITROP-85 (February 1985), M77/3 (January 2009), Callao Time Series Transect (October 2011), M90 (November 2012), M91 (December 2012), AT26-26 (January 2015). The ONI of these years (1985, 2009, 2011, 2012, Figure 1) indicated that, 1985 and 2011 are considered as weak “La Niña” years, whereas 2009 and 2012 are considered “neutral” years. [The MEMENTO database has not archived any N<sub>2</sub>O datasets in the ETSP region during previous El Niño events](#), and therefore we were not able to compare N<sub>2</sub>O dynamics between two El Niño time-periods. To facilitate the comparison, the 2015 and archived N<sub>2</sub>O depth profiles were compared at three offshore and three coastal locations, each within a grid space of 0.75° × 0.75° (see supplementary Table S1 for station coordinates). [Standard deviation of repeated N<sub>2</sub>O concentration measurements \(analytical precision\) for archived N<sub>2</sub>O concentration datasets were retrieved from respective references \(see supplementary Table S1\)](#). These analytical precisions are < 5% of N<sub>2</sub>O concentration values.

### 3 Results

#### 3.1 Hydrography, distribution of oxygen and inorganic nitrogen

The 2015-16 El Niño event impacted the ETSP with a relatively high sea surface temperature anomaly, especially at the equatorial region (2°S – 2°N and 80° – 90°W) where the highest anomaly between 3 and 5 °C was observed at offshore waters (Figure 2a). The El Niño-induced warming effect decreased southwards. Between 5°S and 12°S, the temperature anomaly was 2 – 3 °C. South of 12°S the anomaly was generally < 1 °C. The shelf areas between 7°S and 14°S had a progressively lower temperature anomaly southwards; > 1.5 °C and < 1 °C north and south of 12°S, respectively.

Five water masses, based on their thermohaline indices (Strub et al., 1998; Silva et al., 2009) were identified (Figure 2b). The northward-flowing Antarctic Intermediate water (AAIW, T = 3 – 5 °C, S ≈ 34.5) was found at depths below 1000 m. The Equatorial subsurface water (ESSW, T = 8 – 12 °C, S = 34.7 – 34.9) was near the Peruvian coast at depths between 300 and 400 m. Above the continental slope (water depth < 250 m), the colder Peru coastal water (PCW, T < 19°C, S ≈ 35) occupied 30 – 250 m, whereas the warmer subtropical surface water (STSW, T > 18.5 °C, S > 34.9) was found at depth < 30 m. The surface water north of the equator consisted of the tropical surface water (TSW), which had high temperature and low salinity (T > 25 °C, S < 33.5) due to excess precipitation. The October 2015 water column below 250 m had similar thermohaline properties compared to those of October – December 2012 (non-El Niño) that had been shown in an earlier study (Kock et al., 2016), except that October 2015 had 2 – 4°C warmer surface water.

Along the offshore section, the upper oxycline boundary ([O<sub>2</sub>] = 20 μmol L<sup>-1</sup> isoline) was at 250 – 300 m along the equator at 85.5°W, and the ODZ ([O<sub>2</sub>] < 5 μmol L<sup>-1</sup>) appeared near 10°S (Figure 3a). The southward shoaling of the oxycline, thickening of the ODZ and shoaling of the [NO<sub>3</sub><sup>-</sup>] = 20 μmol L<sup>-1</sup> isoline were observed south of 10°S (Figure 3a and 3b), where the thickness of the ODZ was ~ 300 m. The top of the ODZ reached ~125 m between 13°S and 16°S.

Significant accumulation of  $\text{NO}_2^-$  ( $>1 \mu\text{mol L}^{-1}$ ) occurred south of  $10^\circ\text{S}$  between 30 and 400 meters within the ODZ (Figure 3c), corresponding to lower  $\text{NO}_3^-$  concentrations (Figure 3b). The highest  $\text{NO}_2^-$  concentration ( $9.4 \mu\text{mol L}^{-1}$ ) was recorded at 200 m at  $15.7^\circ\text{S}$ .

Along the coastal section, the surface (upper 10 m)  $\text{O}_2$  concentrations were below saturation at all sampling stations (50 – 97 % saturation). Surface  $\text{O}_2$  concentrations were  $165 - 217 \mu\text{mol L}^{-1}$  north of  $10^\circ\text{S}$  and gradually decreased to  $135 - 190 \mu\text{mol L}^{-1}$  between  $10^\circ\text{S}$  and  $12.5^\circ\text{S}$ , and to  $120 \mu\text{mol L}^{-1}$  south of  $14^\circ\text{S}$  (Figure 3d). The shoaling of the  $[\text{O}_2] = 20 \mu\text{mol L}^{-1}$  isoline was observed south of  $9^\circ\text{S}$ . The top of the ODZ was found at 200 m, 150 m and 80 m at  $11^\circ\text{S}$ ,  $12^\circ\text{S}$  and  $14^\circ\text{S}$ , respectively. The surface  $\text{NO}_3^-$  concentrations were  $11 - 23 \mu\text{mol L}^{-1}$  between  $9^\circ\text{S}$  and  $16^\circ\text{S}$ , and the  $[\text{NO}_3^-] = 20 \mu\text{mol L}^{-1}$  isoline was at 0 – 20 m (Figure 3e). Water column  $\text{NO}_2^-$  concentrations at coastal stations were generally below  $1 \mu\text{mol L}^{-1}$ , with the exception of the station at  $14.0^\circ\text{S}$  where  $\text{NO}_2^-$  concentrations reached  $1.2 \mu\text{mol L}^{-1}$  below 200 m (Figure 3f).

### 3.2 Water column $\text{N}_2\text{O}$ concentrations and isotopes

Along the offshore section, the water column  $\text{N}_2\text{O}$  distributions showed a southward increase of surface concentrations and southward decrease of subsurface concentration maxima (Figure 4a). The equatorial region ( $1^\circ\text{N}$  to  $2.5^\circ\text{S}$ ,  $85.5^\circ\text{W}$ ) had subsurface  $\text{N}_2\text{O}$  concentrations up to  $93 \text{ nmol L}^{-1}$  at thermocline depths (200 – 550 m); water column  $\delta^{15}\text{N}$ , SP and  $\delta^{18}\text{O}$  generally increased with depth (Figure 4b, 4c and 4d); at the subsurface  $\text{N}_2\text{O}$  concentration maximum,  $\delta^{15}\text{N}$ , SP and  $\delta^{18}\text{O}$  were  $\sim 6 \text{ ‰}$ ,  $13 - 17 \text{ ‰}$ , and  $45 - 50 \text{ ‰}$ , respectively. Two  $\text{N}_2\text{O}$  concentration maxima were observed at stations south of  $10^\circ\text{S}$  where the ODZ was formed. Near  $10^\circ\text{S}$ , two  $\text{N}_2\text{O}$  concentration maxima ( $70 \pm 6 \text{ nmol L}^{-1}$ ) occurred between 200 and 600 m; and a local concentration minimum ( $\sim 30 \text{ nmol L}^{-1}$ ) occurred within the ODZ at 400 m, associated with high  $\delta^{15}\text{N}$  ( $8 - 10 \text{ ‰}$ ), SP ( $20 - 30 \text{ ‰}$ ) and  $\delta^{18}\text{O}$  ( $60 - 70 \text{ ‰}$ ). Near  $13^\circ\text{S}$ , a shallow  $\text{N}_2\text{O}$  concentration maximum ( $\sim 80 \text{ nmol L}^{-1}$ ) occurred at  $\sim 100 \text{ m}$ , and a local  $\text{N}_2\text{O}$  concentration minimum ( $18 \text{ nmol L}^{-1}$ ) occurred at 350 m. Between  $14^\circ\text{S}$  and  $16^\circ\text{S}$ , the lowest ( $< 10 \text{ nmol L}^{-1}$ )  $\text{N}_2\text{O}$  concentrations were observed at 200 – 400 m within the ODZ, where the highest values of  $\delta^{15}\text{N}$  ( $> 10 \text{ ‰}$ ), SP ( $30 - 40 \text{ ‰}$ ) and  $\delta^{18}\text{O}$  ( $> 60 \text{ ‰}$ ) were observed.

Along the coastal section, a southward increase of surface  $\text{N}_2\text{O}$  concentration ( $20 \text{ nmol L}^{-1}$  north of  $11^\circ\text{S}$  and  $> 40 \text{ nmol L}^{-1}$  south of  $13^\circ\text{S}$ ) was observed, coinciding with southward shoaling of the ODZ (Figure 4e). Subsurface maximum  $\text{N}_2\text{O}$  concentrations were observed below 200 m near  $10.7^\circ\text{S}$ , and at 80 – 90 m south of  $12^\circ\text{S}$ , where ODZ was formed. The  $\delta^{15}\text{N}$  in coastal waters were between 2.5 and 5 ‰, with lower values at stations south of  $14^\circ\text{S}$  (Figure 4f). SP was lower ( $-10 - 0 \text{ ‰}$ ) at the surface ( $< 10 \text{ m}$ ) near  $9^\circ\text{S}$  and at 50 – 150 m near  $11^\circ\text{S}$ ; higher SP ( $10 - 20 \text{ ‰}$ ) was observed south of  $14^\circ\text{S}$  (Figure 4g). The  $\delta^{18}\text{O}$  values were 45 – 60 ‰; higher  $\delta^{18}\text{O}$  ( $> 55 \text{ ‰}$ ) were observed within the ODZ below 200 m at  $14^\circ\text{S}$  and below 100 m at  $15.3^\circ\text{S}$  (Figure 4h).

### 3.3 Excess N<sub>2</sub>O and N<sub>2</sub>O flux to the atmosphere

Both the offshore and coastal stations showed N<sub>2</sub>O supersaturation in the top 10 m of surface water, and coastal stations had higher  $\Delta\text{N}_2\text{O}$  concentrations (15 – 50 nmol L<sup>-1</sup>) than those of offshore stations (4 – 8 nmol L<sup>-1</sup>). Subsurface  $\Delta\text{N}_2\text{O}$  along the offshore section had higher concentrations at the equatorial regions (70 – 80 nmol L<sup>-1</sup>) than  $\Delta\text{N}_2\text{O}$  concentrations at stations located south of 10 °S (40 – 60 nmol L<sup>-1</sup>, Figure 5a). Near 15 °S, subsurface N<sub>2</sub>O undersaturation was observed;  $\Delta\text{N}_2\text{O}$  concentrations were -4 – 0 nmol L<sup>-1</sup> at thermocline depths (200 – 400 m) within the ODZ ([O<sub>2</sub>] < 5  $\mu\text{mol L}^{-1}$ ). Along the coastal section, a southward increase of surface and subsurface (50 – 200 m)  $\Delta\text{N}_2\text{O}$  was observed (Figure 5b). Subsurface maximum  $\Delta\text{N}_2\text{O}$  concentrations were > 60 nmol L<sup>-1</sup>, and occurring at the periphery of ODZ (~ 200 m near 10 °S and < 100 m south of 12 °S). Undersaturation of N<sub>2</sub>O ( $\Delta\text{N}_2\text{O} < 0$ ) did not occur in any coastal stations. The N<sub>2</sub>O fluxes from the coastal stations were 23 – 108  $\mu\text{mol m}^{-2} \text{d}^{-1}$ , nearly two folds of the offshore fluxes (7 – 50  $\mu\text{mol m}^{-2} \text{d}^{-1}$ , Figure 5c). The highest flux occurred at a coastal station at 14.4°S, 77.3°W, coinciding with the highest surface  $\Delta\text{N}_2\text{O}$  (50 nmol L<sup>-1</sup>).

## 4 Discussion

The ETSP is one of the world's major oceanic OMZs having active N<sub>2</sub>O production and intense efflux to the atmosphere (Arévalo-Martínez et al., 2015; Kock et al., 2016). The gradient spanning from fully oxygenated conditions to anoxia creates suitable conditions for N<sub>2</sub>O production and consumption, which causes the co-existence of water column N<sub>2</sub>O supersaturation and undersaturation (Codispoti and Christensen, 1985). To identify the N<sub>2</sub>O cycling pathways, we input N<sub>2</sub>O isotopic and isotopomeric measurements into a simple mass balance model (section 4.1). Quantitative relationships linking O<sub>2</sub>, NO<sub>3</sub><sup>-</sup> and N<sub>2</sub>O were examined to characterize the effect of oxygenation on N<sub>2</sub>O production from NH<sub>4</sub><sup>+</sup> oxidation (section 4.2). Previously measured N<sub>2</sub>O concentrations from the ETSP were extracted from the MEMENTO database (Kock and Bange, 2015) and were compared to data from this study to investigate the contrasting water column N<sub>2</sub>O distribution and effluxes between El Niño and non-El Niño years (section 4.3), which would better constrain the natural variability of N<sub>2</sub>O cycling in the ETSP.

### 4.1 N<sub>2</sub>O cycling pathways inferred from natural abundance isotopic and isotopomeric signatures

The analyses of natural abundance isotopomers quantify the substitutions of nitrogen and oxygen isotopes occurring on the linear asymmetric N<sub>2</sub>O molecule (Yoshida and Toyoda, 2000), and can be used to identify potential production and consumption pathways (Yamagishi et al., 2007; Grundle et al., 2017). The production of N<sub>2</sub>O in an isolated water body follows mass conservation of the respective isotopes and isotopomers. The mass balance model proposed by Fujii et al. (2013) quantified the isotopic signature of N<sub>2</sub>O produced within the water mass ( $\delta_{\text{produced}}$ ) by the linear regression of the inverse N<sub>2</sub>O concentration ( $1/[\text{N}_2\text{O}]_{\text{measured}}$ ) and the observed isotope values ( $\delta_{\text{observed}}$ ):

$$\delta_{observed} = \frac{1}{[N_2O]_{measured}} \times (\delta_{initial} - \delta_{produced}) \times [N_2O]_{initial} + \delta_{produced} \quad (6)$$

where  $[N_2O]_{initial}$  and  $\delta_{initial}$  refer to source water  $N_2O$  concentration and isotopic signature, respectively. It has been shown that SP is only determined by  $N_2O$  cycling pathways, and that SP is independent of nitrogen isotopic values of the substrates for  $N_2O$  cycling. Both culture and field studies demonstrated that  $N_2O$  production via  $NH_4^+$  oxidation and partial denitrification (including both nitrifier- and denitrifier-mediated denitrification) are associated with typical SP values of  $30 \pm 5$  ‰ and  $0 \pm 5$  ‰, respectively (Toyoda et al., 2011). Recent results from culture (Winther et al., 2018) and river water (Mothet et al., 2013) showed that  $N_2O$  production via denitrification had SP values as low as -10 ‰. Thus, by determining  $SP_{produced}$ ,  $N_2O$  cycling processes can be qualitatively characterized. We further identified four water bodies (coastal and offshore stations combined) from shallow to deeper depths with distinctive features such as  $O_2$ ,  $NO_2^-$  concentrations and depths (Table 1) to discuss  $N_2O$  cycling pathways as follows.

(1) Upper oxycline and surface (Figure S1a):  $[O_2] > 20 \mu mol L^{-1}$ ,  $[NO_2^-] < 1 \mu mol L^{-1}$ , and depth  $< 200$  m.  $N_2O$  production from this water body could actively contribute to atmospheric efflux. The samples had variable SP values (-9 – 34 ‰); some coastal samples had low SP values (-5 to -9 ‰, Figure 4g), which as outlined above is characteristic of strong denitrifying  $N_2O$  production. The low  $SP_{produced}$  ( $6.4 \pm 1.9$ ) indicates that both nitrification and denitrification were sources of  $N_2O$  to the upper oxycline, with the majority appearing to come from denitrification. Given that the  $O_2$  concentrations were too high for denitrification to proceed locally in the upper oxycline and the surface (Codispoti and Christensen, 1985), the SP signature of  $N_2O$  in this water body was a mixture of local nitrification and denitrification signal from the peak  $N_2O$  concentration depths (see below) as a result of active upwelling and upward diffusion in the ETSP (Haskell et al., 2015). Thus, denitrification and nitrification both contribute to  $N_2O$  effluxes in the ETSP-OMZ, consistent with a previous study which focused on the coastal regions between  $\sim 12 - 14^\circ S$  (Bourbonnais et al., 2017).

(2)  $N_2O$  peak (Figure S1b):  $[O_2] = 5 - 20 \mu mol L^{-1}$  and  $[NO_2^-] < 1 \mu mol L^{-1}$ , and depth = 45 – 500 m. The samples were from  $N_2O$  concentration maxima near the upper boundary of the ODZ. The  $SP_{produced}$  is relatively low ( $8.3 \pm 3.0$  ‰) at this suboxic water body ( $[O_2] < 20 \mu mol L^{-1}$ ), which allowed  $N_2O$  production from denitrification while inhibited  $N_2O$  consumption (Bonin et al., 1989; Farías et al., 2009). The  $SP_{produced}$  leads us to conclude that water column  $N_2O$  maximum was mainly attributed to partial denitrification (i.e.  $NO_2^-$  and  $NO_3^-$  reduction). This is consistent with previous  $^{15}N$  tracer incubation experiments demonstrating that  $N_2O$  concentration maximum above the ODZ was likely the result of high rates of  $N_2O$  production from  $NO_2^-$  and  $NO_3^-$  reduction that are 10 – 100 fold higher than the rate of  $NH_4^+$  oxidation to  $N_2O$  (Ji et al., 2015).

(3) Oxygen deficient zone (Figure S1c):  $[O_2] < 5 \mu mol L^{-1}$  and  $[NO_2^-] > 1 \mu mol L^{-1}$ , and depth = 70 – 400 m. The ODZ has prominent features such as the accumulation of  $NO_2^-$  (Codispoti and Christensen, 1985), and undersaturation of  $N_2O$  as a result of dynamic balance between the concomitant  $N_2O$  production (Ji et al., 2015) and consumption by denitrification (Babbin et al., 2015). The isotopic signature of “produced  $N_2O$ ” had distinctively high  $\delta^{15}N_{bulk}$  (8.5 ‰), and



$\delta^{18}\text{O}$  (71 ‰, Table 1 and Figure S2), and this is indicative of pronounced  $\text{N}_2\text{O}$  reduction to  $\text{N}_2$  which results in an isotope enrichment of the remaining  $\text{N}_2\text{O}$  pool in the process of N-O bond breakage (Toyoda et al., 2017). The SP signature was also high (39.9 ‰). While  $\text{NH}_4^+$  oxidation can produce  $\text{N}_2\text{O}$  with similar SP values, we rule this out given the observed low  $\text{O}_2$  concentrations (Peng et al., 2016). Instead, similar to the high  $\delta^{15}\text{N}_{\text{bulk}}$  and  $\delta^{18}\text{O}$  values which were observed, we suggest that the high SP values which were recorded in the ODZ, where  $\text{N}_2\text{O}$  undersaturation occurred, were also a result of  $\text{N}_2\text{O}$  consumption, as reduction of  $\text{N}_2\text{O}$  can also result in high SP values (Popp et al., 2002; Well et al., 2005; Mothet et al., 2013). Based on the observed  $\delta^{15}\text{N}_{\text{bulk}}$ ,  $\delta^{18}\text{O}$  and SP values of  $\text{N}_2\text{O}$ , we conclude that  $\text{N}_2\text{O}$  consumption was the predominant  $\text{N}_2\text{O}$  cycling pathway in the water body with  $[\text{O}_2] < 5 \mu\text{mol L}^{-1}$  and  $[\text{NO}_2^-] > 1 \mu\text{mol L}^{-1}$  in the ETSP.

(4) Intermediate waters (Figure S1d): Samples from depths 500 – 1000 m with  $[\text{O}_2] = 5 - 70 \mu\text{mol L}^{-1}$  and  $[\text{NO}_2^-] < 1 \mu\text{mol L}^{-1}$ . Generally, the  $\text{N}_2\text{O}$  concentration peak below the ODZ at the offshore waters can be found in this water body (Figure 4a). From the linear regression, the  $\text{SP}_{\text{produced}}$  is  $15.6 \pm 4.1$  ‰, indicating that both nitrification- and denitrification-produced  $\text{N}_2\text{O}$  under the oxic and suboxic conditions ( $[\text{O}_2] = 5 - 70 \mu\text{mol L}^{-1}$ ). Downward mixing and diffusion from ODZ is unlikely because the ETSP is a major upwelling region and ODZ samples had high SP values (see next paragraph). We conclude that localized  $\text{N}_2\text{O}$  production from nitrification and denitrification are important pathways in this region of the water column, and probably contributed to  $\text{N}_2\text{O}$  concentrations maxima in intermediate waters, as reported by Carrasco et al. (2017).

There are some limitations of the isotopomers-based analysis of potential  $\text{N}_2\text{O}$  cycling pathways. (1) Constant atmospheric exchange at the surface and mixed layer, and mesoscale eddy activities at intermediate waters (Arévalo-Martínez et al., 2016) could affect the  $\text{SP}_{\text{produced}}$  from localized  $\text{N}_2\text{O}$  cycling. Nevertheless, our conclusion of denitrification being important pathway remains valid. As a comparison, water bodies were divided by potential density surfaces (i.e.  $\sigma_\theta > 27 \text{ kg m}^{-3}$ ,  $26 - 27 \text{ kg m}^{-3}$ ,  $25 - 26 \text{ kg m}^{-3}$ ,  $< 25 \text{ kg m}^{-3}$ ) and showing  $\text{SP}_{\text{produced}}$  of  $5.0 - 11.1$  ‰. (2) We are not able to investigate the change of  $\text{N}_2\text{O}$  production rates from nitrification and denitrification that are affected by El Niño-induced lower export production, as demonstrated by Espinoza-Morriberón et al. (2017). With complimentary dataset such as isotopic compositions of  $\text{NO}_3^-$  and  $\text{NO}_2^-$ , the rates of  $\text{N}_2\text{O}$  production can be derived by isotopic relationships during  $\text{N}_2\text{O}$  production processes using a three dimensional biogeochemical model (Bourbonnais et al., 2017).

#### 4.2 The effect of $\text{O}_2$ on $\text{N}_2\text{O}$ production from $\text{NH}_4^+$ oxidation

The surface and upper oxycline directly contribute to oceanic  $\text{N}_2\text{O}$  effluxes, with  $\text{NH}_4^+$  oxidation being the dominant production pathway due to  $\text{O}_2$  inhibition of denitrification (see section 4.1). Thus, it is worth investigating  $\text{N}_2\text{O}$  production from  $\text{NH}_4^+$  oxidation occurring along the oxygen gradient. During  $\text{NH}_4^+$  oxidation to  $\text{NO}_2^-$ , the effectiveness of  $\text{N}_2\text{O}$  production can be quantified with the  $\text{N}_2\text{O}$  yield, which is defined as the molar nitrogen ratio of  $\text{N}_2\text{O}$  produced and  $\text{NH}_4^+$  oxidized. In oxygenated waters, the near absence of  $\text{NH}_4^+$  and  $\text{NO}_2^-$  suggest the amount of  $\text{NH}_4^+$  oxidized produces equal amounts of  $\text{NO}_3^-$  within measurement error. Rees et al. (2011) and Grundle et al. (2012) computed the  $\text{N}_2\text{O}$  yield by deriving the slope of the linear regression of  $\Delta\text{N}_2\text{O}$ - $\text{NO}_3^-$  relationship. The  $\Delta\text{N}_2\text{O}$  data from all sampling stations during October 2015

showed that  $\Delta\text{N}_2\text{O}$  increases with increasing  $\text{NO}_3^-$  concentrations and decreasing  $\text{O}_2$  concentrations (Figure 6). The samples from the upper oxycline ( $[\text{O}_2] > 20 \mu\text{mol L}^{-1}$  and depth  $< 500 \text{ m}$ ) showed moderate increase of  $\Delta\text{N}_2\text{O}$  ( $0 - 20 \text{ nmol L}^{-1}$ ) when  $[\text{NO}_3^-] < 20 \mu\text{mol L}^{-1}$ . At  $[\text{NO}_3^-] > 20 \mu\text{mol L}^{-1}$ , substantial increase of  $\Delta\text{N}_2\text{O}$  ( $20 - 75 \text{ nmol L}^{-1}$ ) was observed. Here, to avoid sampling the ODZ where suboxic condition stimulates  $\text{N}_2\text{O}$  production from partial denitrification (i.e. water body (3) described in section 4.1), only data from the upper oxycline (depth  $< 500 \text{ m}$ ) were used to perform linear regression. The slope of the regression at  $[\text{NO}_3^-] < 20 \mu\text{mol L}^{-1}$  (corresponding to  $[\text{O}_2] > 100 \mu\text{mol L}^{-1}$ ) is  $0.85 \pm 0.11$ , indicating that  $0.085 \pm 0.011 \text{ nmol}$  of  $\text{N}_2\text{O}$  is produced for every  $\mu\text{mol}$  of  $\text{NO}_3^-$  produced (or  $\text{NH}_4^+$  oxidized), equating to a molar nitrogen yield (mol  $\text{N}_2\text{O-N}$  produced / mol  $\text{NO}_3^-$  produced) of  $0.17 \pm 0.02 \%$ . At  $[\text{NO}_3^-] > 20 \mu\text{mol L}^{-1}$  (corresponding to  $[\text{O}_2] < 100 \mu\text{mol L}^{-1}$ ) the yield increases to  $0.85 \pm 0.13 \%$ .

These  $\text{N}_2\text{O}$  yield estimates are generally comparable to previously reported values ( $0.04 - 1.6 \%$ ) in the ETSP (Elkins et al., 1978; Ji et al., 2015), and indicate that potential  $\text{N}_2\text{O}$  production from  $\text{NH}_4^+$  oxidation decreases with water column oxygenation due to intrusion of oxygen-rich water masses (Llanillo et al., 2013; Graco et al., 2017), as well as El Niño-induced oxygenation (see section 4.3). As discussed earlier, the oxycline samples were probably influenced by mixing of suboxic water with active denitrification producing high  $\text{N}_2\text{O}$  concentrations and low  $\text{NO}_3^-$  concentrations; the  $\text{N}_2\text{O}$  yield estimates here are thus spatially and temporally integrated. As a comparison,  $^{15}\text{N}$  tracer incubation method directly measured  $0.04 \%$   $\text{N}_2\text{O}$  yield during  $\text{NH}_4^+$  oxidation at  $[\text{O}_2] > 100 \mu\text{mol L}^{-1}$  (Ji et al., 2015).

### 4.3 $\text{N}_2\text{O}$ distribution and fluxes during El Niño

Excess  $\text{N}_2\text{O}$  ( $\Delta\text{N}_2\text{O}$ ) in surface waters is one of the principal factors regulating sea-to-air  $\text{N}_2\text{O}$  fluxes. To evaluate the effect of strong El Niño on oceanic  $\text{N}_2\text{O}$  fluxes, we compare surface and water column  $\Delta\text{N}_2\text{O}$  concentrations in shelf waters ( $< 300 \text{ m}$  depth) along  $8 - 16^\circ\text{S}$  during El Niño (October 2015) and “neutral” conditions (December 2012). In the ETSP, Higher surface  $\Delta\text{N}_2\text{O}$  concentrations and thus higher potential  $\text{N}_2\text{O}$  efflux occurred at near-shore waters. Generally, the surface  $\Delta\text{N}_2\text{O}$  concentrations in October 2015 (Figure 7a) were lower than those of December 2012 (Figure 7d); highest surface  $\Delta\text{N}_2\text{O}$  concentrations were  $50$  and  $250 \text{ nmol L}^{-1}$  in 2015 and 2012, respectively. The region of high surface  $\Delta\text{N}_2\text{O}$  occurred at near  $\sim 14^\circ\text{S}$  and  $\sim 10^\circ\text{S}$  in 2015 and in 2012, respectively. It appears that  $\text{N}_2\text{O}$  efflux was significantly reduced during El Niño; in October 2015, coastal water had  $\text{N}_2\text{O}$  flux of  $23 - 108 \mu\text{mol m}^{-2} \text{ d}^{-1}$  (Figure 5c), much lower than that of December 2012 having  $459 - 1825 \mu\text{mol m}^{-2} \text{ d}^{-1}$  (Arévalo-Martínez et al., 2015). Such a  $75 - 95 \%$  reduction in  $\text{N}_2\text{O}$  fluxes during the 2015-16 El Niño in the ETSP was comparable to an 80% reduction in fluxes observed in the central equatorial Pacific during the 1982-83 El Niño (Cline et al., 1987).

Suppressed upwelling or increased downwelling during El Niño events, as observed in both observational and model studies (Llanillo et al., 2013; Graco et al., 2017; Mogollón and Calil, 2017), can directly and indirectly affect  $\text{N}_2\text{O}$  fluxes to the atmosphere: First, reduced upward transport of subsurface  $\text{N}_2\text{O}$ -rich water not only decreased surface  $\Delta\text{N}_2\text{O}$ , but also increased subsurface  $\Delta\text{N}_2\text{O}$ , which is illustrated by the comparative observation of higher subsurface  $\Delta\text{N}_2\text{O}$  concentrations in coastal waters in October 2015 (Figure 7b, 7c) than those in December 2012 (Figure 7e, 7f). Second, because the oxygen

sensitivity of the denitrification sequence increases with each step (Körner and Zumft, 1989), El Niño-induced water column oxygenation inhibited N<sub>2</sub>O consumption within the ODZ (bounded by [O<sub>2</sub>] = 5 μmol L<sup>-1</sup> isoline), as demonstrated by the disappearance of N<sub>2</sub>O undersaturation ( $\Delta N_2O < 0$ ) in coastal water in 2015 (Figure 7b, 7c), contrasting to water column N<sub>2</sub>O undersaturation occurring at 100 m at 13 – 14 °S in December 2012 (Figure 7e, 7f). Third, as shown in this study, the deepening and expansion of the suboxic zone ([O<sub>2</sub>] = 5 – 20 μmol L<sup>-1</sup>) caused by the El Niño event stimulated subsurface N<sub>2</sub>O production via denitrification, as demonstrated by the close spatial coupling between local maximum  $\Delta N_2O$  concentrations and the oxycline ([O<sub>2</sub>] = 5 and 20 μmol L<sup>-1</sup> isolines, Figure 7b and 7e). Lastly, upwelling of oxygen-rich water along the Peruvian coast, especially north of 12 °S (Stramma et al., 2016), inhibited local N<sub>2</sub>O production and caused the southward relocation of surface  $\Delta N_2O$  “hot spots”.

The decrease of surface  $\Delta N_2O$  concentration during El Niño was associated with an increase of subsurface N<sub>2</sub>O concentrations. Water column  $\Delta N_2O$  concentration profiles at expanded temporal and spatial coverage (see Figure 2a for location map, and Table S1 for coordinates) were compared within the same season between El Niño and non-El Niño years (Figure 8). We included N<sub>2</sub>O data from January 2015 when the highest ONI was recorded during austral summer (Figure 1). These comparisons at offshore stations were made to cover the depth ranges with pronounced El Niño effects and available data (1000 m at station A and 800 m at station B and C). At coastal stations the depth ranges were station bottom depth (station D and E) or 250 m (station F). Generally, subsurface  $\Delta N_2O$  concentration peaks were observed at deeper depths during 2015. Offshore stations had higher subsurface peak  $\Delta N_2O$  concentrations during El Niño (Figure 8a, 8b), except at station C where the peak concentration during October 2015 was comparable to that of December 2012 (Figure 8c). At coastal stations D and E, higher  $\Delta N_2O$  concentrations were found below 50 m but peak  $\Delta N_2O$  concentrations were lower during El Niño years (Figure 8d, 8e). In the southernmost coastal station F, the peak  $\Delta N_2O$  concentration was higher in 2015 than that of 1985; both were found at similar depths at ~ 60 m. The increase of subsurface N<sub>2</sub>O concentrations during El Niño resulted in OMZ water column retaining larger amount of N<sub>2</sub>O, as shown by higher depth-integrated N<sub>2</sub>O concentrations during El Niño years than non-El Niño years in both coastal and offshore waters (Figure 9).

In all, the apparent decrease in N<sub>2</sub>O efflux during strong El Niño events in the tropical Pacific, as shown in this study and others (Cline et al., 1987; Butler et al., 1989) is the result of complex physical and biochemical changes. The above comparative analyses are simple due to limited data availability. Consequently, these following aspects are yet to be resolved: (1) It is unclear how offshore N<sub>2</sub>O fluxes vary from “neutral” to El Niño years. Current  $\Delta N_2O$  profiles show higher surface  $\Delta N_2O$  concentrations at station A and B in 2015 (Figure 8a and 8b), whereas the surface  $\Delta N_2O$  was lower in 2015 at station C (Figure 8c). A zonal (east-west) section near 12 °S showed slightly higher offshore surface  $\Delta N_2O$  in 2015 (~ 5 nmol L<sup>-1</sup>, Figure 7c) than in 2012 (~ 1 nmol L<sup>-1</sup>, Figure 7f). The decrease in coastal N<sub>2</sub>O fluxes during El Niño could be compensated by increase in offshore fluxes. (2) The southward relocation of high surface  $\Delta N_2O$  from neutral to El Niño years (Figure 7a and 7d) possibly results in higher surface  $\Delta N_2O$  hence higher N<sub>2</sub>O flux in southern region of ETSP (e.g. south of 16 °S, Figure 8f). (3) Complex hydrographical changes during the El Niño event resulted in the deepening of the ODZ boundary and the depths of peak N<sub>2</sub>O concentration. It is possible that these chemical features occur in the similar

potential density surfaces (with respect to non-El Niño conditions) that are deepened during El Niño, or they occur in different potential density surfaces during El Niño; or a combination of both. (4) It is possible that once the normal upwelling is resumed after the El Niño event, N<sub>2</sub>O produced and retained in the subsurface layer in coastal and offshore waters could be a potential reservoir contributing to high N<sub>2</sub>O fluxes. (5) The co-occurrence of El Niño and mesoscale eddy formation along the Peruvian coast will have complicated effects on N<sub>2</sub>O fluxes, which remains unexplored.

## 5 Conclusions

The Eastern Tropical South Pacific is a major oceanic upwelling region with N<sub>2</sub>O effluxes and active water column production affected by strong El Niño events. During a developing strong El Niño event in October 2015, a more pronounced warming effect occurred at lower latitudes in the ETSP. In comparison to conditions in December 2012 (non-El Niño), deepening of the oxygen deficient zone's upper boundary occurred at coastal waters in October 2015, coinciding with lower peak N<sub>2</sub>O concentrations at deeper depths. Shelf N<sub>2</sub>O effluxes were significantly lower during the 2015 El Niño as a result of lower surface levels of N<sub>2</sub>O supersaturation. However, a change of upwelling pattern appeared to cause higher subsurface N<sub>2</sub>O concentrations and increased the water column N<sub>2</sub>O inventories during El Niño than in other non-El Niño years. Natural abundance isotopic and isotopomeric analysis indicated that both nitrification and denitrification are important pathways for N<sub>2</sub>O production, and denitrification-derived N<sub>2</sub>O [near the suboxic waters](#) probably contributes to the efflux to the atmosphere. Decreased N<sub>2</sub>O efflux and subsurface accumulation during strong El Niño events is likely the result of suppressed upwelling and [a decrease of water column oxygen consumption](#). The current dataset represents a 'snapshot' of a developing El Niño event that lasted 18 months, thus the complex spatial and temporal patterns of El Niño-induced N<sub>2</sub>O distribution in ETSP remain to be explored.

## Figures and tables

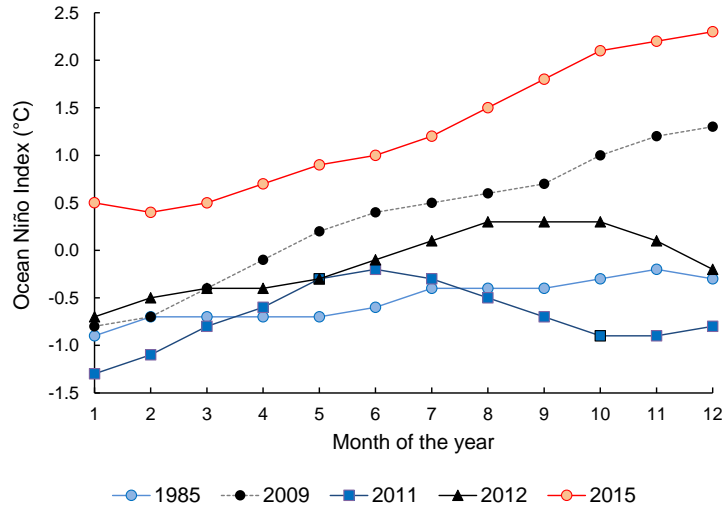


Figure 1: Ocean Niño Index of year 1985 (weak La Niña), 2009 (neutral), 2011 (weak La Niña), 2012 (neutral) and 2015 (strong El Niño). Data was downloaded from:

5 [http://origin.cpc.ncep.noaa.gov/products/analysis\\_monitoring/ensostuff/ONI\\_v5.php](http://origin.cpc.ncep.noaa.gov/products/analysis_monitoring/ensostuff/ONI_v5.php).

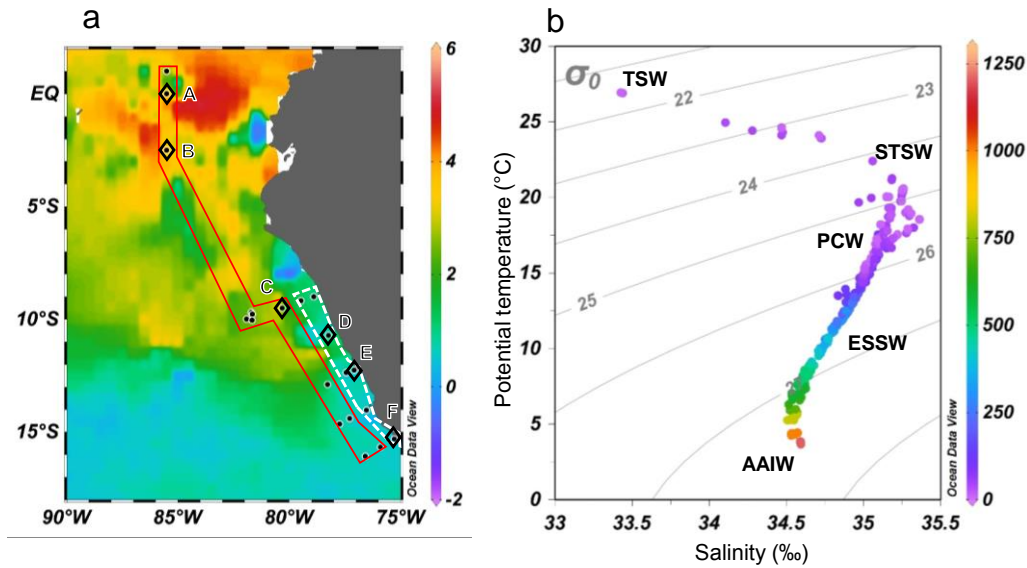


Figure 2: (a) Monthly mean sea surface temperature anomaly ( $^{\circ}\text{C}$ ) of October 2015 from NOAA's Satellite Coral Bleaching Monitoring Datasets. Sampling stations (filled circles) are categorized as "offshore" (in red polygon) and "coastal" sections (in white polygon). Comparative analyses of water column  $\text{N}_2\text{O}$  (see section 4.3) were performed at stations A – E (open diamonds). (b) Potential temperature – salinity diagram, with corresponding depths (meters, colour bar on right) and potential density ( $\sigma_{\theta}$ ,  $\text{kg m}^{-3}$ ) of all sampling stations. Five water masses are shown: Tropical surface water (TSW), Subtropical surface water (STSW), Peru coastal water (PCW), Equatorial subsurface water (ESSW) and Antarctic intermediate water (AAIW).

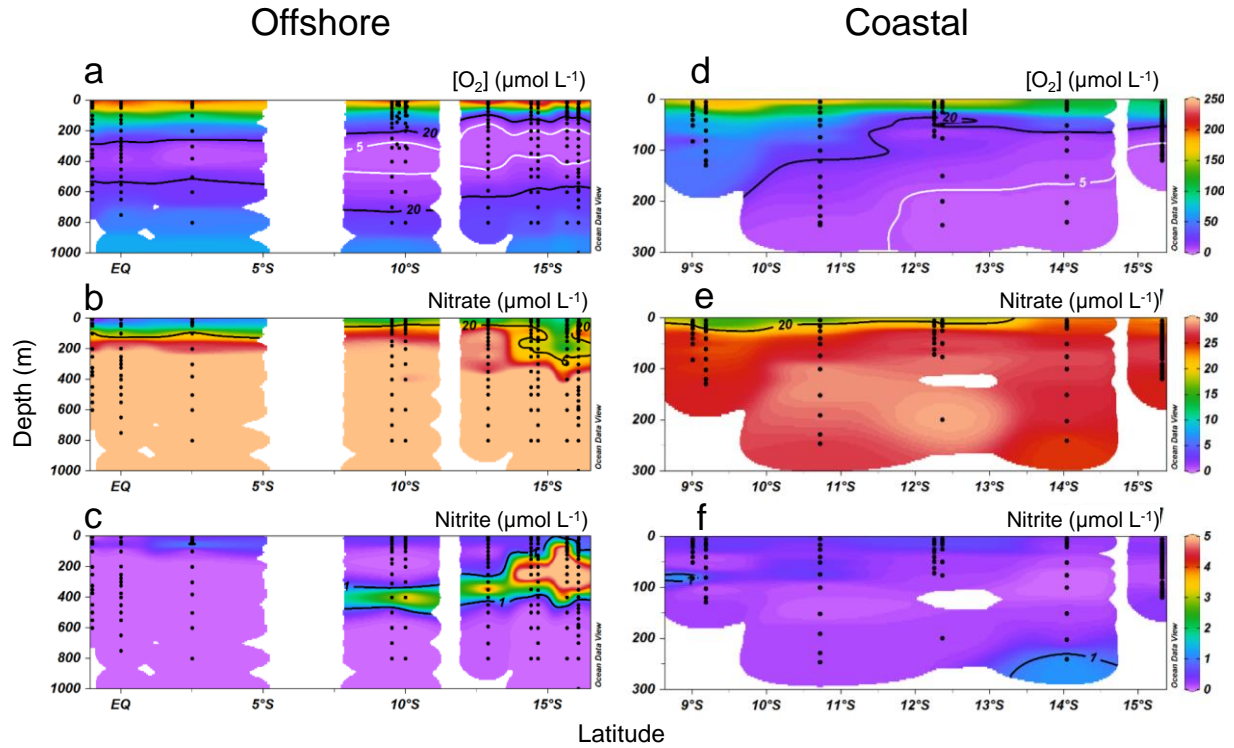
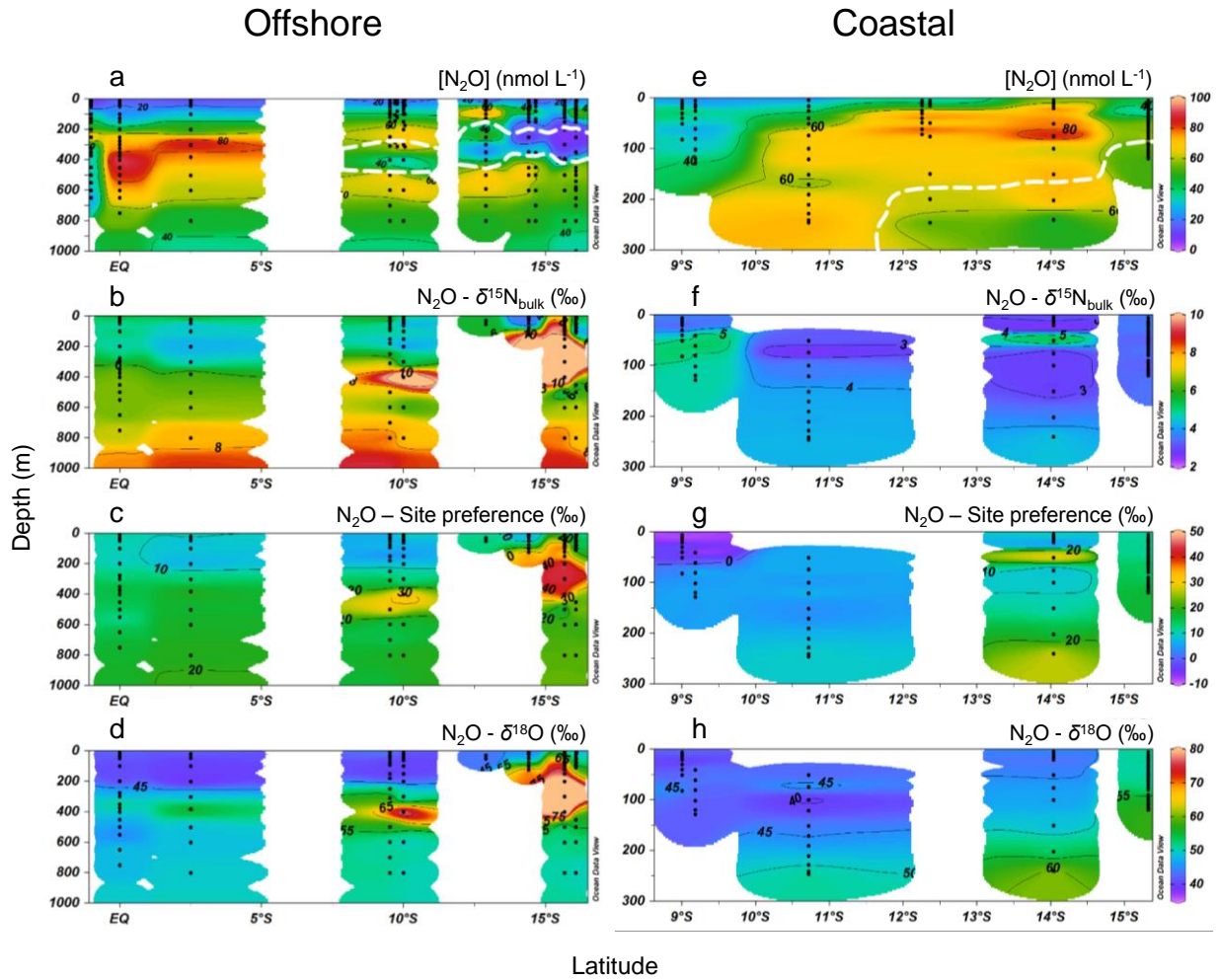
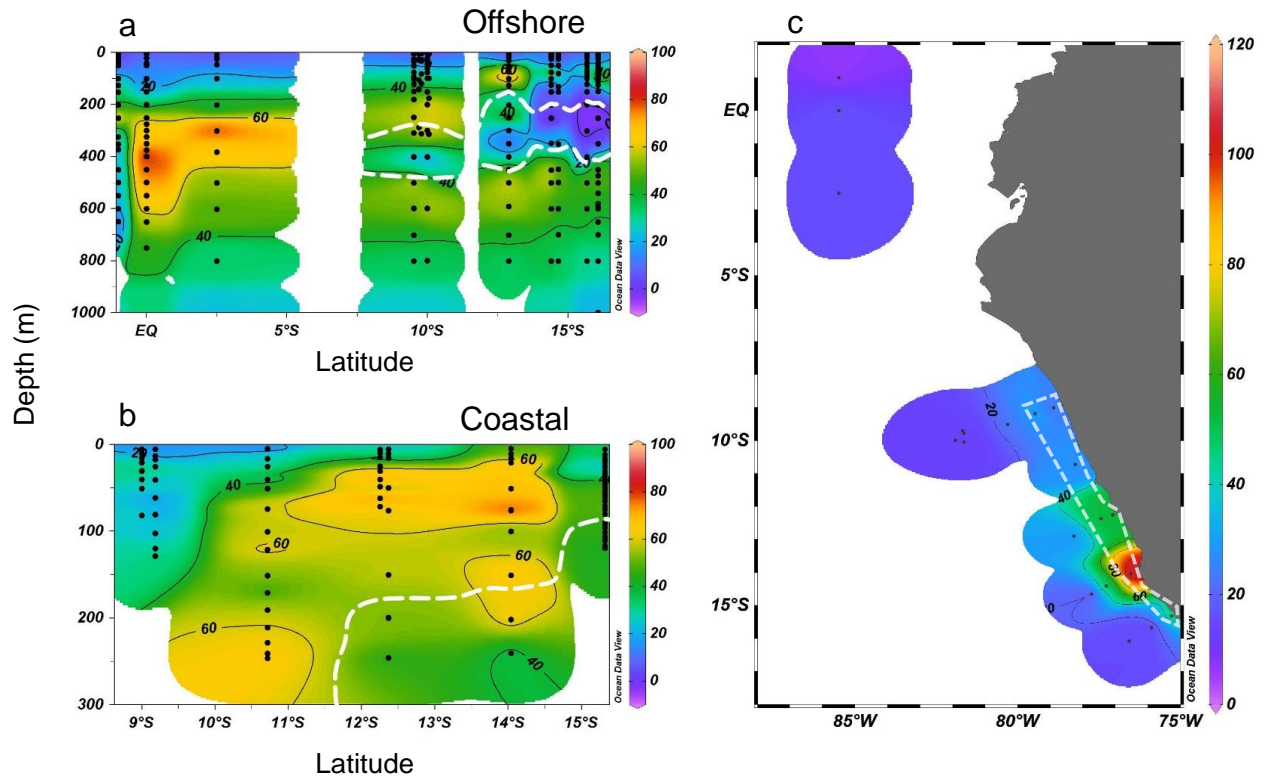


Figure 3: Water column oxygen (a and d), nitrate (b and e) and nitrite concentrations (c and f) along the offshore (a, b and c) and coastal sections (d, e and f) during October 2015.



**Figure 4:** Water column N<sub>2</sub>O concentrations (a and e),  $\delta^{15}\text{N}_{\text{bulk}}$  (b and f), site preference (c and g) and  $\delta^{18}\text{O}$  (d and h) along the offshore (a, b, c and d) and coastal sections (e, f, g and h) during October 2015. White contour line in (a) and (e) denote the boundary of oxygen deficient zone ( $[\text{O}_2] = 5 \mu\text{mol L}^{-1}$  isoline).





**Figure 5: N<sub>2</sub>O excess ( $\Delta N_2O$ , nmol L<sup>-1</sup>) at the offshore section (a) and the coastal section (b) during October 2015; the white dashed line indicates the boundary of the oxygen deficient zone ([O<sub>2</sub>] = 5  $\mu$ mol L<sup>-1</sup> isoline). (c) Surface N<sub>2</sub>O efflux ( $\mu$ mol m<sup>-2</sup> d<sup>-1</sup>) from offshore and coastal stations (enclosed in white polygon) during October 2015.**



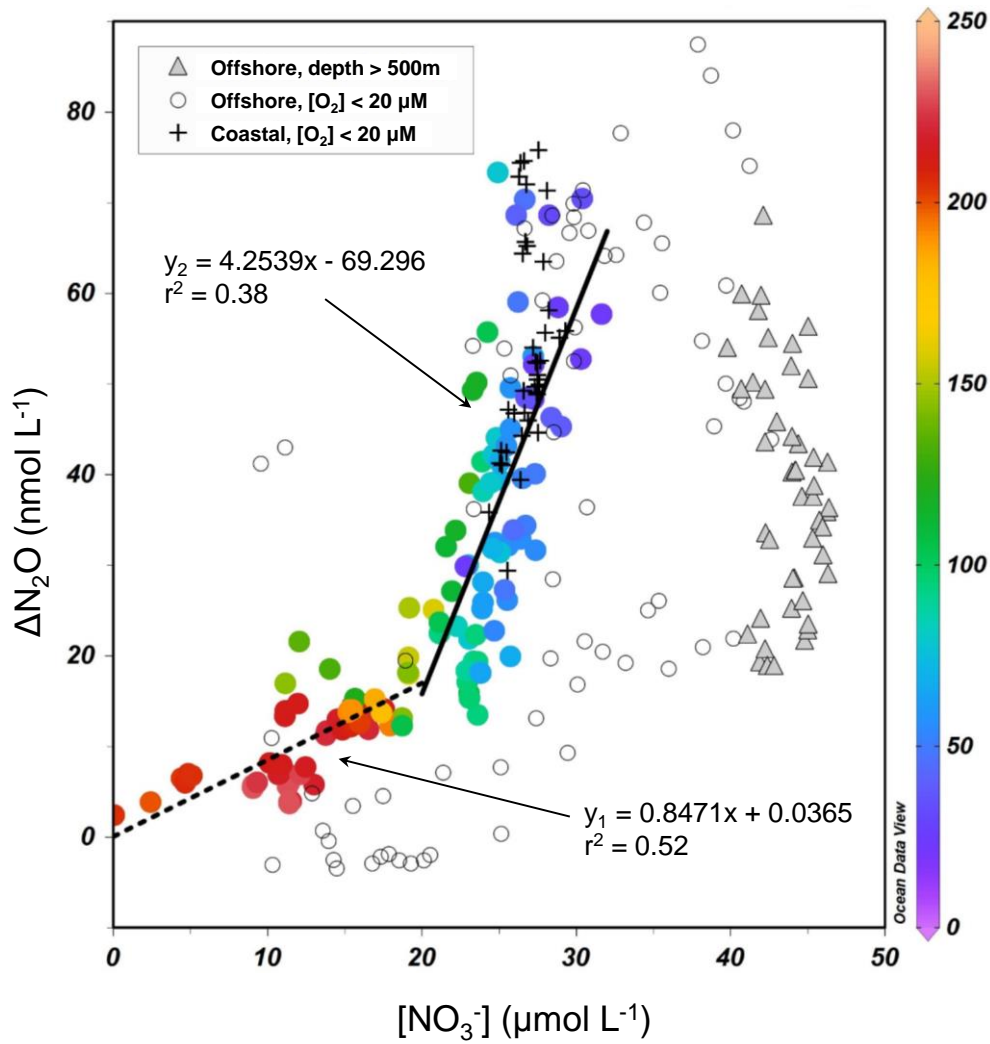


Figure 6:  $\text{NO}_3^-$ - $\Delta\text{N}_2\text{O}$  relationship for samples from the upper oxycline ( $[\text{O}_2] > 20 \mu\text{mol L}^{-1}$ , depth < 500 m, colored circles), low oxygen ( $[\text{O}_2] < 20 \mu\text{mol L}^{-1}$ ) coastal waters (+), low oxygen offshore waters (open circles), and the lower oxycline (depth > 500 m, filled triangles). Color bar shows the  $\text{O}_2$  concentrations ( $\mu\text{mol L}^{-1}$ ). For samples with  $\text{NO}_3^-$  concentrations higher and lower than  $20 \mu\text{mol L}^{-1}$ , two linear regressions were performed separately.

October 2015

December 2012

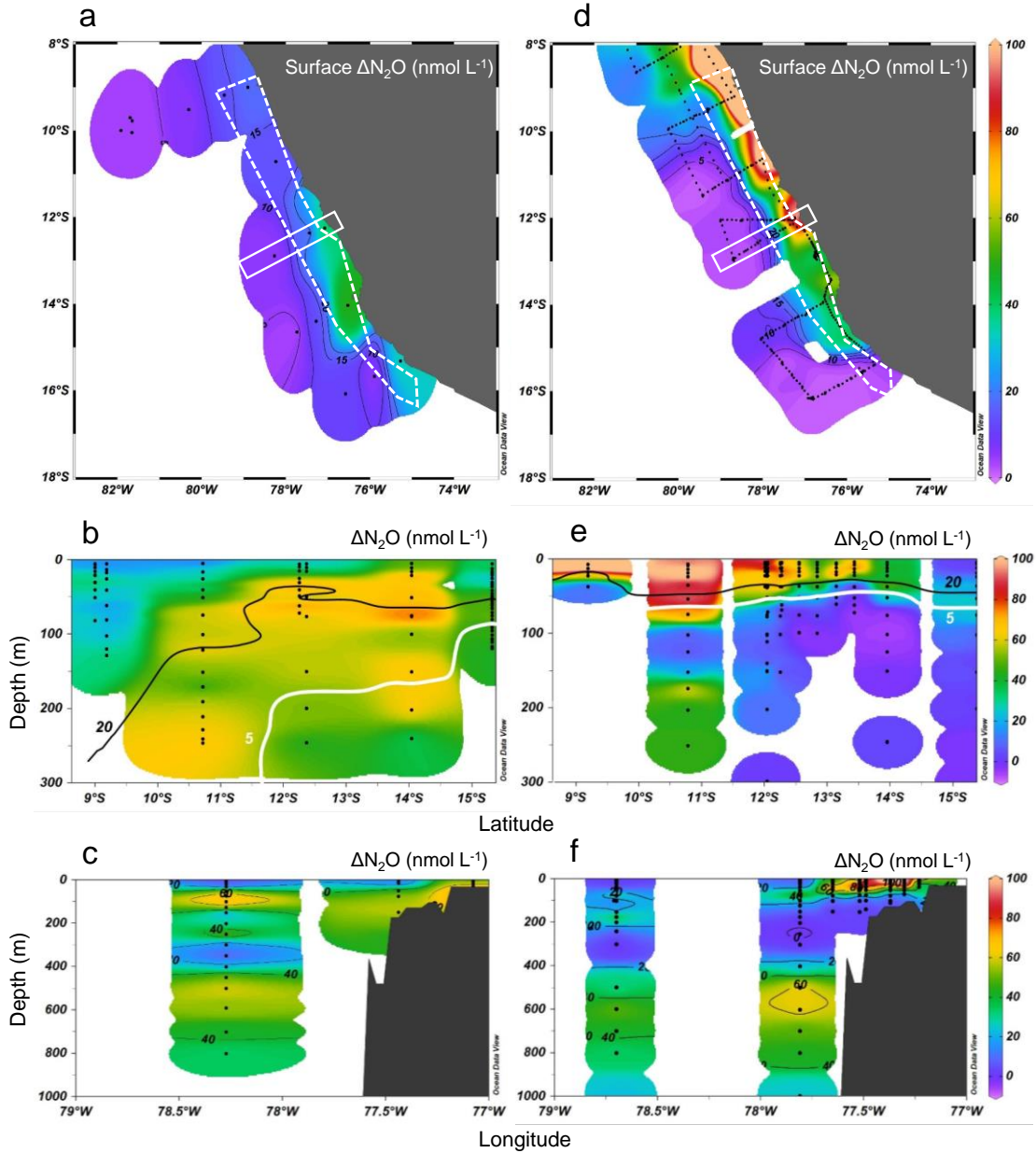
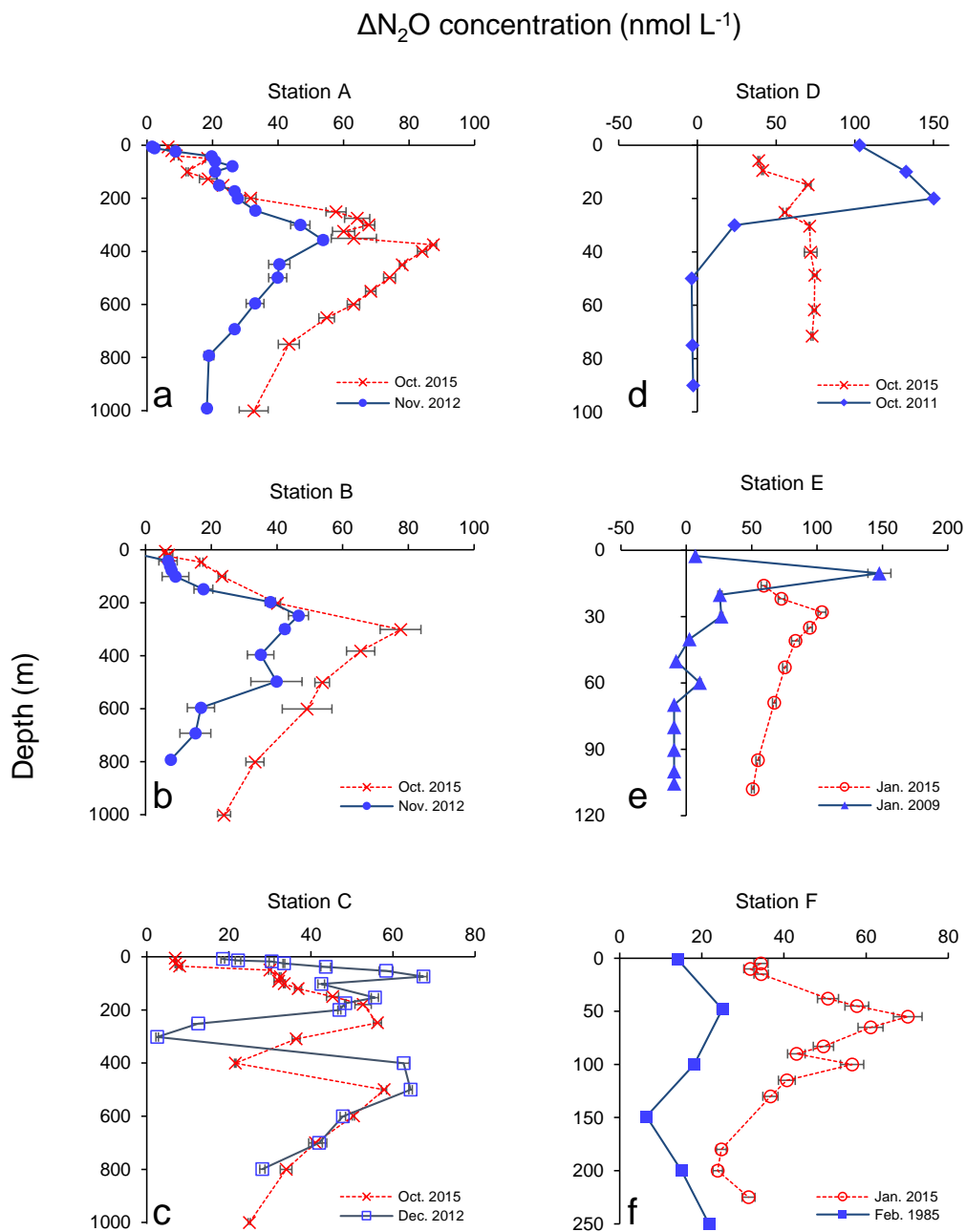


Figure 7: Surface  $\Delta N_2O$  (a and d), meridional water column  $\Delta N_2O$  distribution (b and e) and zonal water column  $\Delta N_2O$  distribution (c and f) in October 2015 and in December 2012. Color bars for  $\Delta N_2O$  (nmol L<sup>-1</sup>) are shown in d, e and f. For meridional  $\Delta N_2O$  distribution (b and e), data are from the coastal section, shown as white dashed polygon in panel (a) and (d). For zonal  $\Delta N_2O$  distribution (c and f), data are from a section 12 – 13°S, shown as white rectangle. In (b) and (e) the “20” contour line (black) denotes the  $[O_2] = 20 \mu\text{mol L}^{-1}$  isoline, equivalent to the lower boundary of oxygenated layer; the “5” contour line (white) denotes the  $[O_2] = 5 \mu\text{mol L}^{-1}$  isoline, equivalent to the upper boundary of oxygen deficient zone.



**Figure 8: Depth profiles of  $N_2O$  concentration excess ( $\Delta N_2O$ , nmol L<sup>-1</sup>) measured at 6 different stations representing offshore (a, b and c) and coastal waters (d, e and f) during February 1985 (filled squares in f), January 2009 (filled triangles in e), October 2011 (filled diamonds in d), November 2012 (filled circles in a and b), December 2012 (open squares in c), January 2015 (open circles in e and f) and October 2015 (crosses). Profiles of 2015 are indicated in red and other years in blue. Error bars represent standard deviation of repeated measurements.**

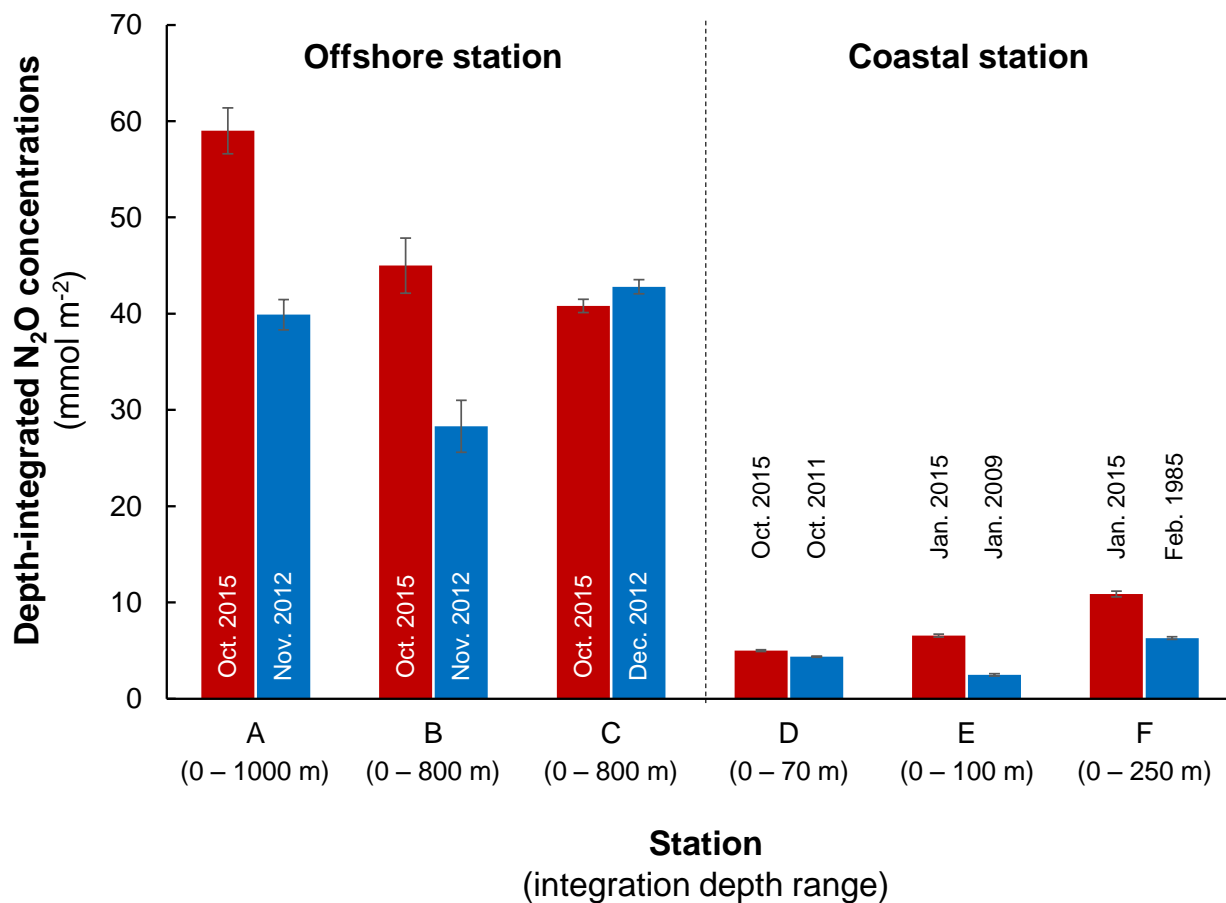


Figure 9 Comparison of depth-integrated  $\text{N}_2\text{O}$  concentrations between El Niño (red bars) and normal years (blue bars). Station A, B and C are characterized as offshore stations whereas D, E and F are as coastal stations. Error bars represent propagation of error from analytical precision of respective  $\text{N}_2\text{O}$  concentration profiles. See Figure 2a for station locations and Table S1 for data sources.

**Table 1: Isotopic signature of N<sub>2</sub>O cycling processes estimated by linear regression of isotopomer ratios and inverse N<sub>2</sub>O concentrations (see section 4.1 for model description and supplementary Figure S1 for results) in water bodies of upper oxycline and surface, N<sub>2</sub>O peak, oxygen deficient zone and intermediate waters.**

No.	Layer	Definition	Statistical properties	$\delta^{15}\text{N}_{\text{bulk}}$ (‰)	$\delta^{18}\text{O}$ (‰)	SP (‰)
1	Upper oxycline and surface	Depth 0 – 200 m	Produced N <sub>2</sub> O	2.8	45.9	6.4
		[O <sub>2</sub> ] > 5 µmol L <sup>-1</sup>	Standard error	0.3	1.2	1.9
		[NO <sub>2</sub> <sup>-</sup> ] < 1 µmol L <sup>-1</sup>	R <sup>2</sup> (n = 76)	0.37	0	0.04
2	N <sub>2</sub> O peak	Depth = 45 – 500 m	Produced N <sub>2</sub> O	5.4	41.3	8.3
		[O <sub>2</sub> ] = 5 – 20 µmol L <sup>-1</sup>	Standard error	0.9	3.0	3.0
		[NO <sub>2</sub> <sup>-</sup> ] < 1 µmol L <sup>-1</sup>	R <sup>2</sup> (n = 48)	0.04	0.24	0.08
3	Oxygen deficient zone	Depth = 70 – 400 m	Produced N <sub>2</sub> O	8.5	71.0	39.9
		[O <sub>2</sub> ] < 5 µmol L <sup>-1</sup>	Standard error	1.5	4.5	4.4
		[NO <sub>2</sub> <sup>-</sup> ] > 1 µmol L <sup>-1</sup>	R <sup>2</sup> (n = 11)	0.38	0.40	0.01
4	Intermediate waters	Depth = 500 – 1000 m	Produced N <sub>2</sub> O	3.6	50.0	15.6
		[O <sub>2</sub> ] = 5 – 70 µmol L <sup>-1</sup>	Standard error	0.6	2.4	4.1
		[NO <sub>2</sub> <sup>-</sup> ] < 0.02 µmol L <sup>-1</sup>	R <sup>2</sup> (n = 21)	0.69	0	0.04

5

### Acknowledgements

The German Federal Ministry of Education and Research (BMBF) grant (03G0243A) awarded to C. Marandino, D. Grundle and T. Steinhoff supported the ASTRA-OMZ cruise onboard the R/V Sonne in October 2015. The German Science Foundation (DFG) provided support via the Collaborative Research Centre 754: Climate-Biogeochemistry Interactions in the Tropical Ocean and funded the R/V Meteor cruises. The BMBF also supported this study as part of the SOPRAN project I and II (03F0611A, 03F0662A). We thank the captains and crews of the R/V Meteor and R/V Sonne cruises for their help, C. Marandino (Chief Scientist) and T. Steinhoff for co-organizing the R/V Sonne cruise with D. Grundle (co-Chief Scientist), and M. Lohmann, H. Campen and M. Sun for the oxygen and nutrient measurements and help with N<sub>2</sub>O sampling. We thank the Peruvian authorities for allowing us to conduct work in their territorial waters. We thank Tina Baustian for contributing hydrography and N<sub>2</sub>O data off the Peruvian coast. In preparation of the manuscript, C. Marandino and L. Stramma provided constructive comments. Ji also received support from DFG grants (GR4731/2-1 and MA6297/3-1) awarded to D. Grundle and C. Marandino.

## Data availability

Raw data presented in this manuscript can be found in the Supplementary material.

## Author contributions

DSG developed the experimental design and was co-PI and co-Chief Scientist of the ASTRA-OMZ cruise. HWB, 5 MIG, XM, DLA-M, and DSG conducted field sampling. DG, MA, XM, DLA-M conducted laboratory analyses. QJ and DSG performed data synthesis. QJ, MA, HWB, MIG, XM, DLA-M, DSG prepared the manuscript.

## Competing Interests

The authors declare that they have no conflict of interest.

## References

- 10 Anderson, J. H.: The metabolism of hydroxylamine to nitrite by *Nitrosomonas*, *The Biochemical Journal*, 91, 8-17, 1964.
- Arévalo-Martínez, D. L., Kock, A., Loscher, C. R., Schmitz, R. A., and Bange, H. W.: Massive nitrous oxide emissions from the tropical South Pacific Ocean, *Nat. Geosci.*, 8, 530-533, <https://doi.org/10.1038/ngeo2469>, 2015.
- 15 Arévalo-Martínez, D. L., Kock, A., Löscher, C. R., Schmitz, R. A., Stramma, L., and Bange, H. W.: Influence of mesoscale eddies on the distribution of nitrous oxide in the eastern tropical South Pacific, *Biogeosciences*, 13, 1105-1118, <https://doi.org/10.5194/bg-13-1105-2016>, 2016.
- 20 Babbin, A. R., Bianchi, D., Jayakumar, A., and Ward, B. B.: Rapid nitrous oxide cycling in the suboxic ocean, *Science*, 348, 1127-1129, <https://doi.org/10.1126/science.aaa8380>, 2015.
- Barber, R. T., and Chavez, F. P.: Biological Consequences of El Niño, *Science*, 222, 1203-1210, <https://doi.org/10.1126/science.222.4629.1203>, 1983.
- 25 Blasing, T.: Recent greenhouse gas concentrations, Carbon Dioxide Information Analysis Center (CDIAC), Oak Ridge National Laboratory (ORNL), Oak Ridge, TN (United States), 2016.
- Bonin, P., Gilewicz, M., and Bertrand, J. C.: Effects of oxygen on each step of denitrification on *Pseudomonas nautica*, *Can. J. Microbiol.*, 35, 1061-1064, <https://doi.org/10.1139/m89-177>, 1989.
- 30 Bourbonnais, A., Letscher, R. T., Bange, H. W., Échevin, V., Larkum, J., Mohn, J., Yoshida, N., and Altabet, M. A.: N<sub>2</sub>O production and consumption from stable isotopic and concentration data in the Peruvian coastal upwelling system, *Glob. Biogeochem. Cycles*, 31, 678-698, <https://doi.org/10.1002/2016GB005567>, 2017.
- 35 Butler, J. H., Elkins, J. W., Thompson, T. M., and Egan, K. B.: Tropospheric and dissolved N<sub>2</sub>O of the west Pacific and east Indian Oceans during the El Niño Southern Oscillation event of 1987, *J. Geophys. Res. Atmos.*, 94, 14865-14877, <https://doi.org/10.1029/JD094iD12p14865>, 1989.
- 40 Carrasco, C., Karstensen, J., and Farias, L.: On the Nitrous Oxide Accumulation in Intermediate Waters of the Eastern South Pacific Ocean, *Front. Mar. Sci.*, 4, <https://doi.org/10.3389/fmars.2017.00024>, 2017.

- Chavez, F. P., Ryan, J., Lluch-Cota, S. E., and Ñiquen C., M.: From Anchovies to Sardines and Back: Multidecadal Change in the Pacific Ocean, *Science*, 299, 217-221, <https://doi.org/10.1126/science.1075880>, 2003.
- 5 Cline, J. D., Wisegarver, D. P., and Kelly-Hansen, K.: Nitrous oxide and vertical mixing in the equatorial Pacific during the 1982–1983 El Niño, *Deep. Sea. Res.*, 34, 857-873, [https://doi.org/10.1016/0198-0149\(87\)90041-0](https://doi.org/10.1016/0198-0149(87)90041-0), 1987.
- Codispoti, L. A., and Christensen, J. P.: Nitrification, denitrification and nitrous oxide cycling in the eastern tropical South Pacific ocean, *Mar. Chem.*, 16, 277-300, [https://doi.org/10.1016/0304-4203\(85\)90051-9](https://doi.org/10.1016/0304-4203(85)90051-9), 1985.
- 10 Cornejo, M., Murillo, A. A., and Farías, L.: An unaccounted for N<sub>2</sub>O sink in the surface water of the eastern subtropical South Pacific: Physical versus biological mechanisms, *Prog. Oceanogr.*, 137, 12-23, <https://doi.org/10.1016/j.pocean.2014.12.016>, 2015.
- Elkins, J. W., Steven C. Wofsy, Michael B. McElroy, Charles E. Kolb, and Kaplan, W. A.: Aquatic sources and sinks for nitrous oxide, *Nature*, 275, 602-606, <https://doi.org/10.1038/275602a0>, 1978.
- 15 Espinoza-Morriberón, D., Echevin, V., Colas, F., Tam, J., Ledesma, J., Vázquez, L., and Graco, M.: Impacts of El Niño events on the Peruvian upwelling system productivity, *J. Geophys. Res. Oceans*, 122, 5423-5444, <https://doi.org/10.1002/2016JC012439>, 2017.
- 20 Farías, L., Castro-González, M., Cornejo, M., Charpentier, J., Faúndez, J., Boontanon, N., and Yoshida, N.: Denitrification and nitrous oxide cycling within the upper oxycline of the eastern tropical South Pacific oxygen minimum zone, *Limnol. Oceanogr.*, 54, 132-144, <https://doi.org/10.4319/lo.2009.54.1.0132>, 2009.
- 25 Farías, L., Faúndez, J., Fernández, C., Cornejo, M., Sanhueza, S., and Carrasco, C.: Biological N<sub>2</sub>O Fixation in the Eastern South Pacific Ocean and Marine Cyanobacterial Cultures, *PLOS ONE*, 8, e63956, <https://doi.org/10.1371/journal.pone.0063956>, 2013.
- Frame, C. H., and Casciotti, K. L.: Biogeochemical controls and isotopic signatures of nitrous oxide production by a marine ammonia-oxidizing bacterium, *Biogeosciences*, 7, 2695-2709, <https://doi.org/10.5194/bg-7-2695-2010>, 2010.
- 30 Fujii, A., Toyoda, S., Yoshida, O., Watanabe, S., Sasaki, K. i., and Yoshida, N.: Distribution of nitrous oxide dissolved in water masses in the eastern subtropical North Pacific and its origin inferred from isotopomer analysis, *Journal of Oceanography*, 69, 147-157, <https://doi.org/10.1007/s10872-012-0162-4>, 2013.
- 35 Garcia, H. E., and Gordon, L. I.: Oxygen solubility in seawater: Better fitting equations, *Limnol. Oceanogr.*, 6, 1307-1312, <https://doi.org/10.4319/lo.1992.37.6.1307>, 1992.
- Graco, M. I., Purca, S., Dewitte, B., Castro, C. G., Morán, O., Ledesma, J., Flores, G., and Gutiérrez, D.: The OMZ and nutrient features as a signature of interannual and low-frequency variability in the Peruvian upwelling system, *Biogeosciences*, 14, 4601-4617, <https://doi.org/10.5194/bg-14-4601-2017>, 2017.
- 40 Grundle, D. S., Maranger, R., and Juniper, S. K.: Upper Water Column Nitrous Oxide Distributions in the Northeast Subarctic Pacific Ocean, *Atmos. Ocean*, 50, 475-486, <https://doi.org/10.1080/07055900.2012.727779>, 2012.
- 45 Grundle, D. S., Löscher, C. R., Krahmann, G., Altabet, M. A., Bange, H. W., Karstensen, J., Körtzinger, A., and Fiedler, B.: Low oxygen eddies in the eastern tropical North Atlantic: Implications for N<sub>2</sub>O cycling, *Sci. Rep.*, 7, 4806, <https://doi.org/10.1038/s41598-017-04745-y>, 2017.
- Haskell, W. Z., Kadko, D., Hammond, D. E., Knapp, A. N., Prokopenko, M. G., Berelson, W. M., and Capone, D. G.: Upwelling velocity and eddy diffusivity from 7Be measurements used to compare vertical nutrient flux to export POC flux in the Eastern Tropical South Pacific, *Mar. Chem.*, 168, 140-150, <https://doi.org/10.1016/j.marchem.2014.10.004>, 2015.
- 50 Ji, Q., Babbín, A. R., Jayakumar, A., Oleynik, S., and Ward, B. B.: Nitrous oxide production by nitrification and denitrification in the Eastern Tropical South Pacific oxygen minimum zone, *Geophys. Res. Lett.*, 42, 10,755-710,764, <https://doi.org/10.1002/2015GL066853>, 2015.
- 55 Kock, A., and Bange, H. W.: Counting the ocean's greenhouse gas emissions, *Eos*, 10-13, <https://doi.org/10.1029/2015EO023665>, 2015.

- Kock, A., Arevalo-Martinez, D. L., Löscher, C., and Bange, H. W.: Extreme N<sub>2</sub>O accumulation in the coastal oxygen minimum zone off Peru, *Biogeosciences*, 13, 827-840, <https://doi.org/10.5194/bg-13-827-2016>, 2016.
- 5 Kärner, H., and Zumft, W. G.: Expression of denitrification enzymes in response to the dissolved oxygen level and respiratory substrate in continuous culture of *Pseudomonas stutzeri*, *Appl. Environ. Microbiol.*, 55, 1670-1676, 1989.
- Llanillo, P. J., Karstensen, J., Pelegrí J. L., and Stramma, L.: Physical and biogeochemical forcing of oxygen and nitrate changes during El Niño/El Viejo and La Niña/La Vieja upper-ocean phases in the tropical eastern South Pacific along 86°W, *Biogeosciences*, 10, 6339-6355, <https://doi.org/10.5194/bg-10-6339-2013>, 2013.
- 10 Mogollán, R., and Calil, P. H. R.: On the effects of ENSO on ocean biogeochemistry in the Northern Humboldt Current System (NHCS): A modeling study, *Journal of Marine Systems*, 172, 137-159, <https://doi.org/10.1016/j.jmarsys.2017.03.011>, 2017.
- Mohn, J., Wolf, B., Toyoda, S., Lin, C.-T., Liang, M.-C., Brüggemann, N., Wissel, H., Steiker Amy, E., Dyckmans, J., Szvec, L., Ostrom Nathaniel, E., Casciotti Karen, L., Forbes, M., Giesemann, A., Well, R., Doucett Richard, R., Yarnes Chris, T., Ridley Anna, R., Kaiser, J., and Yoshida, N.: Interlaboratory assessment of nitrous oxide isotopomer analysis by isotope ratio mass spectrometry and laser spectroscopy: current status and perspectives, *Rapid Commun. Mass Spectrom.*, 28, 1995-2007, <https://doi.org/10.1002/rcm.6982>, 2014.
- 15 Mothet, A., Sebilo, M., Laverman, A. M., Vaury, V., and Mariotti, A.: Is site preference of N<sub>2</sub>O a tool to identify benthic denitrifier N<sub>2</sub>O?, *Environ. Chem.*, 10, 281-284, <https://doi.org/10.1071/EN13021>, 2013.
- 20 Ñiquen, M., and Bouchon, M.: Impact of El Niño events on pelagic fisheries in Peruvian waters, *Deep Sea Res Part 2 Top Stud Oceanogr.*, 51, 563-574, <https://doi.org/10.1016/j.dsr2.2004.03.001>, 2004.
- 25 Peng, X., Fuchsman, C. A., Jayakumar, A., Warner, M. J., Devol, A. H., and Ward, B. B.: Revisiting nitrification in the Eastern Tropical South Pacific: A focus on controls, *J. Geophys. Res. Oceans*, 121, 1667-1684, <https://doi.org/10.1002/2015JC011455>, 2016.
- Philander, S. G. H.: El Nino Southern Oscillation phenomena, *Nature*, 302, 295-301, <https://doi.org/10.1038/302295a0>, 1983.
- 30 Popp, B. N., Westley, M. B., Toyoda, S., Miwa, T., Dore, J. E., Yoshida, N., Rust, T. M., Sansone, F. J., Russ, M. E., Ostrom, N. E., and Ostrom, P. H.: Nitrogen and oxygen isotopomeric constraints on the origins and sea-to-air flux of N<sub>2</sub>O in the oligotrophic subtropical North Pacific gyre, *Glob. Biogeochem. Cycles.*, 16, 12-11-12-10, <https://doi.org/10.1029/2001GB001806>, 2002.
- Ravishankara, A., Daniel, J. S., and Portmann, R. W.: Nitrous oxide (N<sub>2</sub>O): the dominant ozone-depleting substance emitted in the 21st century, *Science*, 326, 123-125, <https://doi.org/10.1126/science.1176985> 2009.
- 35 Rees, A. P., Brown, I. J., Clark, D. R., and Torres, R.: The Lagrangian progression of nitrous oxide within filaments formed in the Mauritanian upwelling, *Geophys. Res. Lett.*, 38, L21606, <https://doi.org/10.1029/2011GL049322>, 2011.
- 40 Revsbech, N. P., Larsen, L. H., Gundersen, J., Dalsgaard, T., Ulloa, O., and Thamdrup, B.: Determination of ultra-low oxygen concentrations in oxygen minimum zones by the STOX sensor, *Limnol Oceanogr. Meth.*, 7, 371-381, <https://doi.org/10.4319/lom.2009.7.371>, 2009.
- Santoso, A., Mcphaden, M. J., and Cai, W.: The defining characteristics of ENSO extremes and the strong 2015/2016 El Niño, *Rev. Geophys.*, 55, 1079-1129, <https://doi.org/10.1002/2017RG000560>, 2017.
- 45 Silva, N., Rojas, N., and Fedele, A.: Water masses in the Humboldt Current System: Properties, distribution, and the nitrate deficit as a chemical water mass tracer for Equatorial Subsurface Water off Chile, *Deep Sea Res Part 2 Top Stud Oceanogr.*, 56, 1004-1020, <https://doi.org/10.1016/j.dsr2.2008.12.013>, 2009.
- 50 Stramma, L., Fischer, T., Grundle, D. S., Krahmann, G., Bange, H. W., and Marandino, C. A.: Observed El Niño conditions in the eastern tropical Pacific in October 2015, *Ocean Sci.*, 12, 861-873, <https://doi.org/10.5194/os-12-861-2016>, 2016.
- Strub, P. T., Mesías, J. M., Montecino, V., Rutillant, J., and Salinas, S.: Coastal ocean circulation off western south America., in: *The Sea*, edited by: Robinson, A. R., and Brink, K. H., John Wiley, New York, 273-313, 1998.
- 55



- Toyoda, S., Yano, M., Nishimura, S.-i., Akiyama, H., Hayakawa, A., Koba, K., Sudo, S., Yagi, K., Makabe, A., Tobari, Y., Ogawa, N. O., Ohkouchi, N., Yamada, K., and Yoshida, N.: Characterization and production and consumption processes of N<sub>2</sub>O emitted from temperate agricultural soils determined via isotopomer ratio analysis, *Glob. Biogeochem. Cycles.*, 25, n/a-n/a, <https://doi.org/10.1029/2009GB003769>, 2011.
- 5 Toyoda, S., Yoshida, N., and Koba, K.: Isotopocule analysis of biologically produced nitrous oxide in various environments, *Mass Spectrom. Rev.*, 36, 135-160, <https://doi.org/10.1002/mas.21459>, 2017.
- 10 Trimmer, M., Chronopoulou, P.-M., Maanoja, S. T., Upstill-Goddard, R. C., Kitidis, V., and Purdy, K. J.: Nitrous oxide as a function of oxygen and archaeal gene abundance in the North Pacific, *Nat. Commun.*, 7, 13451, <https://doi.org/10.1038/ncomms13451>, 2016.
- Walter, S., Breitenbach, U., Bange, H. W., Nausch, G., and Wallace, D. W. R.: Distribution of N<sub>2</sub>O in the Baltic Sea during transition from anoxic to oxic conditions, *Biogeosciences*, 3, 557-570, <https://doi.org/10.5194/bg-3-557-2006>, 2006.
- 15 Wanninkhof, R.: Relationship between wind speed and gas exchange over the ocean revisited, *Limnol Oceanogr. Meth.*, 12, 351-362, <https://doi.org/doi:10.4319/lom.2014.12.351>, 2014.
- Weiss, R. F., and Price, B. A.: Nitrous oxide solubility in water and seawater, *Mar. Chem.*, 8, 347-359, [https://doi.org/10.1016/0304-4203\(80\)90024-9](https://doi.org/10.1016/0304-4203(80)90024-9), 1980.
- 20 Well, R., Flessa, H., Jaradat, F., Toyoda, S., and Yoshida, N.: Measurement of isotopomer signatures of N<sub>2</sub>O in groundwater, *J Geophys. Res. Biogeosci.*, 110, <https://doi.org/10.1029/2005JG000044>, 2005.
- 25 Winther, M., Balslev-Harder, D., Christensen, S., Priemé A., Elberling, B., Crosson, E., and Blunier, T.: Continuous measurements of nitrous oxide isotopomers during incubation experiments, *Biogeosciences*, 15, 767-780, <https://doi.org/10.5194/bg-15-767-2018>, 2018.
- Yamagishi, H., Westley, M. B., Popp, B. N., Toyoda, S., Yoshida, N., Watanabe, S., Koba, K., and Yamanaka, Y.: Role of nitrification and denitrification on the nitrous oxide cycle in the eastern tropical North Pacific and Gulf of California, *J Geophys. Res. Biogeosci.*, 112, n/a-n/a, <https://doi.org/10.1029/2006JG000227>, 2007.
- 30 Yang, S., Gruber, N., Long, M. C., and Vogt, M.: ENSO-Driven Variability of Denitrification and Suboxia in the Eastern Tropical Pacific Ocean, *Glob. Biogeochem. Cycles.*, 31, 1470-1487, <https://doi.org/10.1002/2016GB005596>, 2017.
- 35 Yoshida, N., and Toyoda, S.: Constraining the atmospheric N<sub>2</sub>O budget from intramolecular site preference in N<sub>2</sub>O isotopomers, *Nature*, 405, 330, <https://doi.org/10.1038/35012558>, 2000.